

# GRAPH-INFORMED ADVERSARIAL MODELING: INFIMAL SUBADDITIVITY OF INTERPOLATIVE DIVERGENCES

---

**Panagiota Birmpa**

School of Mathematical and Computer Sciences  
Heriot-Watt University  
Edinburgh EH14 4AS, UK

Maxwell Institute for Mathematical Sciences  
Edinburgh EH8 9BT

P.Birmpa@hw.ac.uk

**Eric Joseph Hall**

School of Mathematical and Computer Sciences  
Heriot-Watt University  
Edinburgh EH14 4AS, UK

Maxwell Institute for Mathematical Sciences  
Edinburgh EH8 9BT

e.hall@hw.ac.uk

## ABSTRACT

We study adversarial learning when the target distribution factorizes according to a known Bayesian network. For interpolative divergences, including  $(f, \Gamma)$ -divergences, we prove a new infimal subadditivity principle showing that, under suitable conditions, a global variational discrepancy is controlled by an average of family-level discrepancies aligned with the graph. In an additive regime, this surrogate is exact. This provides a variational justification for replacing a graph-agnostic GAN with a monolithic discriminator by a graph-informed GAN with localized family-level discriminators. The result does not require the optimizer itself to factorize according to the graph. We also obtain parallel results for integral probability metrics and proximal optimal transport divergences, identify natural discriminator classes for which the theory applies, and present experiments showing improved stability and structural recovery relative to graph-agnostic baselines.

**Keywords:** generative adversarial networks, Bayesian networks, variational learning,  $(f, \Gamma)$ -divergences, infimal subadditivity, structured generative models, multi-discriminator learning

## 1 INTRODUCTION

A Generative Adversarial Network (GAN) (Goodfellow et al., 2014) is an artificial neural network architecture used in learning a probability distribution from a given dataset by generating new data samples that resemble a given dataset. Recent advances in GANs have been driven by a deeper understanding of the underlying probability divergences and distances that govern their training. Frameworks such as  $f$ -GANs (Nowozin et al., 2016) generalize the objective to any  $f$ -divergence, enabling flexible modeling through variational estimation, while Wasserstein GANs (Arjovsky et al., 2017; Gulrajani et al., 2017) reformulate the problem using the Earth Mover’s distance, offering improved gradient behavior and stability via the integral probability metric framework. More recent developments use divergences which interpolate between 1-Wasserstein and Kullback–Leibler (KL) divergence as developed in Dupuis and Mao (2022). This divergence has been extended to  $(f, \Gamma)$ -divergences (Birrell et al., 2022a), a broader family that interpolates between integral probability metrics (IPMs) (Müller, 1997) and  $f$ -divergences, and has been extensively examined for its role in the design and theoretical analysis of generative models, particularly with respect to stability and robustness (Dupuis and Mao, 2022; Birrell et al., 2022a; Chen et al., 2024; Gu et al., 2024). Many other divergences have been developed, for example, see Stein et al. (2024); Terjék (2021); Baptista et al. (2025); Birrell and Ebrahimi (2023); Birrell et al. (2022c).

GANs are often trained without explicitly exploiting known conditional dependence structure in the target distribution. In this paper, we refer to such approaches as *graph-agnostic* when the discrimi-

nator acts on the full joint distribution and does not use a known graphical model constructed from side information. In some applications, however, side information about the distribution is available, such as known physical/chemical laws, covariates, design constraints, and expert judgments. In Feizi et al. (2017) the authors proposed GAN architectures tailored to multivariate Gaussian distributions, while Balaji et al. (2019) and Farnia et al. (2023) extended the analysis to GANs designed for mixtures of Gaussians. Birrell et al. (2022b) introduces structure-preserving GANs which leverage additional structure, such as group symmetry, to learn data-efficiently via new variational representations of divergences. The approach reduces the discriminator space to its projection onto the invariant subspace using conditional expectation with respect to the  $\sigma$ -algebra defined by the structure.

However, in this work we shift our focus to cases where conditional dependencies of variables involved in the model could be represented by a Bayesian network (see Pearl (1988); Koller and Friedman (2009)), e.g., the variables might follow a Markov chain. Formally, a Bayesian network is a joint probability distribution on a collection of random variables indexed by the vertices of a Directed Acyclic Graph (DAG). Let  $G = (V, E)$  be a DAG with vertex set  $V = \{1, \dots, n\}$ ,  $n \in \mathbb{N}$ , and edge set  $E \subseteq V \times V$ . We associate to each vertex  $i \in V$  a random variable  $X_i$  taking values in a space  $\mathcal{X}_i$ , and write  $\mathbf{X} = \mathbf{X}_V = (X_1, \dots, X_n)$  with state space  $\mathcal{X} = \mathcal{X}_1 \times \dots \times \mathcal{X}_n$ . The Bayesian network is then the pair  $(G, P)$ , where the joint distribution  $P$  of  $\mathbf{X}$  factorizes according to  $G$  as

$$P(dx_1, \dots, dx_n) = \prod_{i=1}^n P_{i|\text{Pa}(i)}(dx_i \mid \mathbf{X}_{\text{Pa}(i)} = \mathbf{x}_{\text{Pa}(i)}),$$

where  $\text{Pa}(i)$  denotes the parents of vertex  $i$  and  $P_{i|\text{Pa}(i)}$  are the corresponding conditional probability distributions (CPDs) or marginal distributions if  $\text{Pa}(i) = \emptyset$ . Intuitively, a Bayesian network encodes which variables directly depend on which others, providing a structured factorization of the joint distribution. In this paper, we refer to GANs that explicitly use this graphical information in the design of the discriminator objective as *graph-informed*.

Theoretical foundations for exploiting a known Bayesian network or undirected Markov random field structure to design graph-informed GANs with multiple simple discriminators, each enforcing constraints on local neighborhoods of the Bayesian network or Markov random field, were established in Ding et al. (2021), building on prior results in Daskalakis and Pan (2017). This framework relies on the subadditivity properties of classical measures of discrepancy between probability distributions—such as KL divergence, Jensen–Shannon (JS) divergence, and Wasserstein distance—in the context of Bayesian networks and Markov random fields with or without mild conditions. These properties provide upper bounds on the divergence between two high-dimensional distributions sharing the same graphical structure by expressing it as a sum of divergences between their conditionals/marginals over local neighborhoods. Here and throughout the paper, we use *classical divergences* to refer to unrestricted discrepancy functionals such as  $f$ -divergences, and *interpolative divergences* to refer to discrepancies such as  $(f, \Gamma)$ -divergences, which constrain the discriminator’s function class.

Motivated by these ideas, we establish an analogous variant of the subadditivity property on Bayesian networks, referred to as  $\alpha$ -linear generalized infimal subadditivity. More precisely, for a measure of discrepancy  $\delta$  with respect to measures of discrepancy  $\delta_1, \dots, \delta_n$

$$\inf_{P \in \mathcal{P}(\mathcal{X})} \delta(Q, P) \leq \inf_{P \in \mathcal{P}(\mathcal{X})} \alpha \sum_{i=1}^n \delta_i(Q_{i \cup \text{Pa}(i)}, P_{i \cup \text{Pa}(i)}),$$

for all Bayesian networks  $Q$ , where  $Q_{i \cup \text{Pa}(i)}$   $P_{i \cup \text{Pa}(i)}$  are the marginals of  $Q$  and  $P$  over the  $i$ -th node and its parents. We show that  $(f, \Gamma)$ -divergences and other interpolative divergences satisfy  $\alpha$ -linear generalized infimal subadditivity, whereas classical  $f$ -divergences satisfy  $\frac{1}{n}$ -linear generalized infimal additivity, that is, the case where the above inequality holds with equality.

In generative modeling, a monolithic discriminator acting on a high-dimensional, joint distribution poses both computational and statistical challenges: min–max optimization is costly, and hypothesis testing in high dimensions requires sample complexity that grows exponentially with the dimension. Guided by our main theoretical results, which establish  $\alpha$ -linear generalized infimal (sub)additivity principles for classes of statistical discrepancies, we propose graph-informed training strategies. Our work shows that, when the target has a known Bayesian network structure, a graph-informed GAN can replace a graph-agnostic GAN, achieving computational and statistical advantages.

This paper is organized as follows. In the next section, we place our contribution in the broader literature on structure-aware generative modeling and adversarial learning. In Section 3, we recall the variational approach for learning adversarial generative models and key statistical discrepancies. We introduce localized function classes and conditional expectation operators used to encode the factorization of the target probability distribution with respect to a Bayesian network in Section 4. Our main theoretical results, namely Theorems 5.4, 5.6, and 5.7, which prove infimal subadditivity for  $(f, \Gamma)$ -divergences, IPMs, and optimal transport divergences, are presented in Section 5. These provide guarantees (certificates) for replacing global discrepancy minimization by a principled, graph-informed surrogate. Finally, we present several numerical case studies in Section 6 and discuss implications and future work in Section 7.

## 2 RELATED WORK

Existing work on incorporating structure into adversarial generative modeling can be broadly divided into two strands. The first builds structure directly into the generator architecture or training procedure, for example, through causal mechanisms, fairness constraints, or conditional independence objectives. The second uses multiple discriminators or localized adversarial objectives as a practical strategy for high-dimensional generation, typically without a general variational justification. Our work is closest in spirit to the latter, but differs in that it provides theory and foundations, namely a general graph-informed adversarial learning strategy for interpolative divergences on Bayesian networks, continuing in the spirit of Ding et al. (2021).

Within the first strand, Kocaoglu et al. (2017) were among the first to integrate structural causal models into GANs; in this work, the generator is explicitly designed to reflect an assumed causal graph, making it a pioneering framework for learning causal implicit generative models through adversarial training. Moraffah et al. (2020) propose CAN, a two-stage GAN framework that learns causal structure from data and can generate both conditional and interventional samples by embedding a structural causal model and an intervention mechanism into the adversarial architecture. Wen et al. (2022) proposes Causal-TGAN for tabular data generation, incorporating predefined causal relationships into GANs to enhance data fidelity, while Feng et al. (2022) also studies the incorporation of structural causal elements into generator design. In the fairness literature, Xu et al. (2019) introduces CFGAN, which enforces causal fairness criteria such as total effect and direct/indirect discrimination, and Van Breugel et al. (2021) develops DECAF, a GAN that embeds structural causal models into the generator’s input layers to produce fair synthetic data while capturing the underlying causal mechanisms critical for fairness. Related, Ahuja et al. (2021) proposes a GAN-based framework that generates data distributions close to the original while enforcing conditional independence constraints through an additional adversarial objective, and which directly ensures fairness, and Casajús-Setián et al. (2022) proposes a Bayesian-network autoencoder trained adversarially for interpretable anomaly detection.

These prior studies focus primarily on incorporating structure through the generator, through auxiliary constraints, or through the overall training architecture. That is, they focus on injecting structure through model design. By contrast, our contribution is on the discriminator-side and variational: a general variational principle grounded in a new infimal subadditivity result for  $(f, \Gamma)$ -divergences on distributions with known Bayesian network structure. We study how known Bayesian network structure can be used to replace a graph-agnostic monolithic discriminator objective by graph-informed family-level objectives, and we show that this yields a principled surrogate for the corresponding graph-constrained global discrepancy. Methodologically, this connects to empirical multicritic strategies used, for example, in image-to-image translation methods (Yu et al., 2019), recurrent neural networks and time-series generation (Hyland et al., 2018), convolutional neural networks (Nie et al., 2018), and inpainting (Chang et al., 2019). However, our results supply the missing theoretical rationale for these largely heuristic approaches: when the target factorizes according to a Bayesian network, sums of local graph-informed discrepancies control the corresponding global objective.

A separate but related strand relates to graph-structure generation, where graph-structured and conditional generative models have been explored in You et al. (2018), incorporating relational structure into generation. In the broader context of graph neural networks (GNNs), originally introduced in Scarselli et al. (2008) with earlier foundational ideas appearing in Sperduti and Starita (1997), our work is conceptually related in that both frameworks exploit graph-induced locality to replace a

global high-dimensional learning problem by a collection of structured local operations. In GNNs, this is achieved through message passing and feature aggregation over local neighborhoods. Such architectures have been particularly successful in material science, where graph-based representations naturally encode atomic and molecular interactions; see, for example, Xie and Grossman (2018); Reiser et al. (2022); Du et al. (2024). Furthermore, GNNs equivariant to rotations have been studied in Satorras et al. (2021). By contrast, our approach uses local variational discriminators defined on each node and its parent set in order to control a divergence between full probability models.

Our contribution is not to introduce another architecture-specific mechanism for injecting structure, but to develop a general variational principle for graph-informed adversarial learning. To make this precise, we next review the variational formulation of GAN training and the discrepancy functionals that underpin our later subadditivity and infimal subadditivity results.

### 3 VARIATIONAL LEARNING IN GANS

The purpose of this section is to set out the variational framework and discrepancy functionals used in the remainder of the paper. In particular, we review  $f$ -divergences, IPMs,  $(f, \Gamma)$ -divergences, and proximal optimal transport divergences within a common language that will support the later graph-informed analysis.

GANs are a class of neural architectures for learning probability distributions from data by training a generator to synthesize samples that mimic a target dataset. Training is formulated as a zero-sum game between a generator and a discriminator that compete against each other. Formally, let  $(\mathcal{X}, \mathcal{M})$  be a measurable space and  $\mathcal{P}(\mathcal{X})$  be the space of probability distributions on  $\mathcal{X}$ . For a fixed target distribution  $Q \in \mathcal{P}(\mathcal{X})$ , GAN learning is formulated as a min–max problem for some objective functional  $H : \Gamma \times \mathcal{P}(\mathcal{X}) \times \mathcal{P}(\mathcal{X}) \rightarrow \mathbb{R}$ , i.e.,

$$\inf_{g \in \mathcal{G}} \sup_{\gamma \in \Gamma} H(\gamma; Q, P_g), \quad (1)$$

where  $\mathcal{G}$  and  $\Gamma$  are the spaces of generators and discriminators, respectively, and are parametrized by neural networks. The generator  $g : Z \rightarrow \mathcal{X}$  is a sufficiently expressive mapping that transforms a random noise vector  $z \in Z$ , sampled from a prior distribution  $P_Z$  (e.g., Gaussian or uniform), into a synthetic data point  $g(z) \in \mathcal{X}$  in the same space as the real data. The mapping  $g$  pushes the prior distribution forward to the generated probability distribution  $P_g = P \circ g^{-1}$ , with the aim that  $P_g$  is indistinguishable from the real data,  $Q$ . On the other hand, the discriminator  $\gamma : \mathcal{X} \rightarrow \mathbb{R}$  then attempts to distinguish samples from  $Q$  and  $P_g$ .

#### 3.1 TRAINING VIA VARIATIONAL REPRESENTATIONS

We begin by explaining how the min–max problem in (1) can be interpreted as minimizing a variationally defined discrepancy between probability measures. In most GANs, (1) corresponds to minimizing a measure of discrepancy between the target probability distribution  $Q$  and the generated  $P_g$ . More generally, for any  $P, Q \in \mathcal{P}(\mathcal{X})$ , under suitable choices of the objective functional  $H$  and the function class  $\Gamma$ , the quantity,

$$\mathcal{D}(Q, P; H, \Gamma) = \sup_{\gamma \in \Gamma} H(\gamma; Q, P),$$

can be a divergence, an Integral Probabilistic Metric (IPM), or an optimal transport cost between probability distributions  $Q$  and  $P$ . In this notation, (1) has the representation,

$$\inf_{g \in \mathcal{G}} \sup_{\gamma \in \Gamma} H(\gamma; Q, P_g) = \inf_{g \in \mathcal{G}} \mathcal{D}(Q, P_g; H, \Gamma).$$

However, not every measure of discrepancy possesses the *divergence property*, namely,

$$\mathcal{D}(Q, P; H, \Gamma) = 0 \quad \text{if and only if} \quad Q = P.$$

This property is important from a statistical and optimization perspective because it ensures that achieving zero discrepancy is equivalent to recovering the target distribution itself. In Birrell et al. (2022a), the authors identify sufficient conditions under which this property holds for several examples of such discrepancies, including those considered in this work. For the convenience of the reader, relevant definitions of admissible sets are provided in Appendix A.

The next subsections instantiate this general template for the main discrepancy classes relevant to GAN training and to our later analysis.

### 3.2 $f$ -DIVERGENCES

We begin with  $f$ -divergences, since they provide one of the classical variational formulations used in GAN training and motivate the role of convex conjugates in discriminator objectives. Let  $f : [0, \infty) \rightarrow \mathbb{R}$  be strictly convex and lower semicontinuous with  $f(1) = 0$ . For probability distributions  $P, Q \in \mathcal{P}(\mathcal{X})$ , the  $f$ -divergence of  $Q$  with respect to  $P$  is defined by

$$\mathfrak{D}_f(Q\|P) = E_P \left[ f \left( \frac{dQ}{dP} \right) \right], \quad (2)$$

if  $Q \ll P$ , and set to  $+\infty$  otherwise, where  $dQ/dP$  denotes the Radon–Nikodym derivative. This divergence admits the variational representation,

$$\mathfrak{D}_f(Q\|P) = \sup_{\gamma \in \mathcal{M}_b(\mathcal{X})} \left\{ E_Q[\gamma] - \inf_{\nu \in \mathbb{R}} \{ \nu + E_P[f^*(\gamma - \nu)] \} \right\}, \quad (3)$$

where  $f^*(s) = \sup_{t \in \mathbb{R}} \{ st - f(t) \}$  is the Legendre–Fenchel transform (convex conjugate) of  $f$ . For variational training of GANs, the choice of  $f$  determines both the divergence  $\mathfrak{D}_f(Q\|P)$  and the nonlinearity in the discriminator through its convex conjugate  $f^*$ . In particular, the growth of  $f^*$  controls how strongly large values  $\gamma(x)$  are penalized under the reference distribution  $Q$ .

In the sequel, we will use the KL divergence with  $f_{\text{KL}}(t) = t \log t - t + 1$  and the JS divergence with

$$f_{\text{JS}}(t) = \frac{1}{2} \left[ t \log t - (t + 1) \log \left( \frac{t + 1}{2} \right) \right], \quad t \geq 0.$$

The corresponding Legendre–Fenchel transforms are  $f_{\text{KL}}^*(s) = e^{s-1}$  and  $f_{\text{JS}}^*(s) = -\log(2 - e^s)$ ,  $s < \log 2$  (see, e.g., Nowozin et al. (2016)). In the KL case,  $f_{\text{KL}}^*$  has exponential growth, which heavily penalizes large discriminator values and emphasizes rare events where  $P$  and  $Q$  disagree in the tails. Moreover, for the KL divergence the infimum over  $\nu$  in (3) can be solved analytically and one recovers the classical Donsker–Varadhan representation (cf. (21)), in which the discriminator objective involves a log-moment generating function  $\log E_P[e^\gamma]$  term, a form that underlies many existing  $f$ -GAN and risk-sensitive objectives. Unlike KL, the JS divergence is symmetric and bounded,  $0 \leq \mathfrak{D}_{\text{JS}}(Q\|P) \leq \log 2$ , and the corresponding conjugate  $f_{\text{JS}}^*$  diverges only logarithmically as  $s \rightarrow \log 2$ , so the penalty on extreme discriminator values is much milder than when using KL. In the JS case, the variational representation recovers the original logistic GAN objective (up to an additive constant and a reparameterization of  $\gamma$ ). In our experiments involving discrete Bayesian networks, we therefore focus on the JS divergence, since its symmetry and boundedness (it remains finite even when  $P$  and  $Q$  have partially mismatched support) tend to yield more stable training than KL-based objectives in this setting.

### 3.3 $\Gamma$ -INTEGRAL PROBABILITY METRICS ( $\Gamma$ -IPMS)

We next turn to  $\Gamma$ -IPMs, which arise when the discriminator is constrained to a prescribed function class and include several widely used probability metrics. Let  $\Gamma \subset \mathcal{M}_b(\mathcal{X})$ , a class of bounded measurable test functions on  $\mathcal{X}$ , and the associated  $\Gamma$ -IPM as,

$$W^\Gamma(Q, P) = \sup_{\gamma \in \Gamma} \{ E_Q[\gamma] - E_P[\gamma] \}.$$

Under certain conditions for  $\Gamma \subset \mathcal{M}_b(\mathcal{X})$  (Birrell et al., 2022a, Theorem 8),  $W^\Gamma$  satisfies the divergence property. If  $\Gamma \subset C_b(\mathcal{X})$  is strictly admissible (see Appendix A), then  $W^\Gamma$  also satisfies the divergence property (Birrell et al., 2022a, Theorem 15). Different choices of  $\Gamma$  yield many classical probability metrics, including Wasserstein distances, total variation, the Dudley metric, and the maximum mean discrepancy. In the context of GANs, choosing  $\Gamma$  corresponds to specifying the discriminator function class, and hence determines which IPM is minimized during training.

More generally, taking  $\Gamma = \{ \gamma : \mathcal{X} \rightarrow \mathbb{R} \}$  to be:

1.  $\Gamma = \text{Lip}_b^1(\mathcal{X})$  yields the 1-Wasserstein distance and its variants,
2.  $\Gamma = \{ \gamma \in C_b(\mathcal{X}) : \|\gamma\|_\infty \leq 1 \}$  yields (a multiple of) the total variation distance,
3.  $\Gamma = \{ \gamma \in \text{Lip}_b^1(\mathcal{X}) : \|\gamma\|_\infty \leq 1 \}$  yields the Dudley metric, and

4.  $\Gamma = \{\gamma \in \mathcal{H} : \|\gamma\|_{\mathcal{H}} \leq 1\}$ , i.e., the unit ball in a RKHS  $\mathcal{H} \subset C_b(\mathcal{X})$ , yields a generalization of maximum mean discrepancy.

These examples illustrate how regularity and boundedness constraints on  $\Gamma$  translate into different notions of “distance” between  $Q$  and  $P$ , and hence into different inductive biases in the associated GAN discriminators, determining which discrepancies between  $Q$  and  $P$  are emphasized during training.

### 3.4 $(f, \Gamma)$ -DIVERGENCES

The viewpoints from Sections 3.2 and 3.3 can be combined in the form of  $(f, \Gamma)$ -divergences, which interpolate between  $f$ -divergences and IPMs and will be central to our later results. Recall from (3) that the  $f$ -divergence can be written in variational form as a supremum over all bounded measurable functions. In practice, however, both in statistical estimation and in GAN training, the discriminator is restricted to a smaller function class (Birrell et al., 2022a). Given a convex  $f$  and a class of test functions  $\Gamma \subset \mathcal{M}_b(\mathcal{X})$ , we define the corresponding  $(f, \Gamma)$ -divergence by,

$$\mathfrak{D}_f^\Gamma(Q\|P) = \sup_{\gamma \in \Gamma} \left\{ E_Q[\gamma] - \inf_{\nu \in \mathbb{R}} \{ \nu + E_P[f^*(\gamma - \nu)] \} \right\}, \quad (4)$$

where  $f^*$  is the convex conjugate of  $f$ . When  $\Gamma = \mathcal{M}_b(\mathcal{X})$ , then (4) reduces to the  $f$ -divergence  $D_f(Q\|P)$ . In (Birrell et al., 2022a, Theorem 8), the authors prove that under suitable conditions,  $\mathfrak{D}_f^\Gamma(Q\|P)$  is a divergence, i.e.  $\mathfrak{D}_f^\Gamma(Q\|P) \geq 0$  with equality if and only if  $Q = P$ , and interpolates between  $f$ -divergences and  $\Gamma$ -IPMs via an infimal convolutional formula, i.e.,

$$\mathfrak{D}_f^\Gamma(Q\|P) = \inf_{R \in \mathcal{P}(\mathcal{X})} \{ W^\Gamma(Q, R) + \mathfrak{D}_f(R\|P) \}. \quad (5)$$

In particular, we have  $0 \leq \mathfrak{D}_f^\Gamma(Q\|P) \leq \min \{ \mathfrak{D}_f(Q\|P), W^\Gamma(Q, P) \}$ . In (Birrell et al., 2022a, Theorem 15), the same result is proven when  $\Gamma \subset C_b(\mathcal{X})$  and  $\mathcal{X}$  is a Polish space. In Theorem 25 of the same paper, it is proven that there exists a unique optimizer  $R^* \in \mathcal{P}(\mathcal{X})$  in (5) and there exists an optimizer  $\gamma^* \in \Gamma$  in (4) which is unique (up to a constant) in  $\text{supp}(P) \cap \text{supp}(Q)$ . Moreover  $\gamma^*$  and  $R^*$  satisfy

$$dR^* \propto (f^*)'(\gamma^*)dP, \quad \text{or equivalently} \quad \gamma^* = f' \left( \frac{dR^*}{dP} \right) + \text{constant}, \quad (6)$$

and we have  $W^\Gamma(Q, R^*) = E_Q[\gamma^*] - E_{R^*}[\gamma^*]$ .

We introduce the set  $\Gamma^L = \{L\gamma : \gamma \in \Gamma\}$  for  $L > 0$ . For the  $(f, \Gamma^L)$ -divergence, the optimizers of (4) and (5) depend on  $L$  and consequently change with different choices of  $L$ .

In the GAN setting,  $(f, \Gamma)$ -divergences capture exactly the discrepancy that can be detected by a discriminator constrained to the function class  $\Gamma$  (e.g., a neural network architecture with Lipschitz or locality constraints), and will be the central objects in our subadditivity results for Bayesian network-aligned discriminators.

### 3.5 PROXIMAL OPTIMAL TRANSPORT DIVERGENCES

Finally, we consider proximal optimal transport divergences, which provide an interpolation between transport-based and information-theoretic discrepancies and fit naturally into the variational framework developed above. Proximal optimal transport divergence, introduced in Baptista et al. (2025), is a discrepancy measure that interpolates between information divergences and optimal transport distances via an infimal convolution formulation,

$$\mathfrak{D}_\varepsilon^c(Q\|P) = \inf_R \{ T_c(Q, R) + \varepsilon \mathfrak{D}_f(R\|P) \}, \quad (7)$$

where the infimum is over all probability distributions  $R$  on a Polish space  $\mathcal{X}$  and  $T_c$  is the optimal transport cost corresponding to a cost function  $c : \mathcal{X} \times \mathcal{X} \rightarrow [0, \infty)$ . When  $T_c$  is the 1-Wasserstein distance, then (7) becomes an  $(f, \Gamma)$ -divergence with  $f = f_{\text{KL}}$  and  $\Gamma = \text{Lip}_b^1(\mathcal{X})$ . As in  $(f, \Gamma)$ -divergence the dual formulation offers a variational representation involving test functions. For

example, for  $f = f_{\text{KL}}$  and  $c$  bounded below and lower semicontinuous, the dual representation is given by

$$\mathfrak{D}_{\text{KL},\varepsilon}^c(Q||P) = \sup_{\substack{(\phi,\psi) \in C_b(\mathcal{X}) \times C_b(\mathcal{X}), \\ \phi \oplus \psi \leq c}} \left\{ E_Q[\phi] - \varepsilon \ln E_P[e^{-\psi/\varepsilon}] \right\},$$

where  $\phi \oplus \psi$  denotes the function  $\phi(x) + \psi(y)$ . For general cost functions  $c$ , we cannot expect the optimizers of the optimal transport cost to be bounded, but there exist optimizers  $\phi \in L^1(Q)$  and  $\psi \in L^1(P)$  such that  $\phi \oplus \psi \leq c$ .

Our aim is to exploit the graphical structure arising from side information. When  $Q$  is a target Bayesian network, the discrepancies introduced above do not yet exploit this structural information. In the remainder of the paper, we specialize to distributions that factorize according to Bayesian networks, as described in the next section. In Section 5, we then establish a  $\frac{1}{n}$ -linear infimal sub-additivity property that will allow us to define localized discriminator classes and to relate global objective functionals to lower-dimensional components associated with the graph.

## 4 BAYESIAN NETWORK OPERATORS

We now introduce the Bayesian network framework that provides the structural setting for the variational discrepancies considered in the previous section. Our aim is to encode the factorization of the target probability distribution with respect to a DAG and to define the notation needed for localized function classes and conditional expectation operators. These objects will be used in the sequel to formulate and analyze graph-aligned discriminator objectives.

Continuing the Bayesian network notation from Section 1, for a DAG denoted  $G = (V, E)$ , the random vector  $\mathbf{X} = \mathbf{X}_V = (X_1, \dots, X_n)$  indexed by the vertices  $V$  takes values  $\mathbf{x} = (x_1, \dots, x_n)$  in the state space  $\mathcal{X} = \mathcal{X}_1 \times \dots \times \mathcal{X}_n$ . We denote the joint probability distribution of  $\mathbf{X}$  by  $Q$  (with density  $q$  if it exists). For any subset  $A = \{i_1, \dots, i_m\} \subset V$ , we denote  $\mathbf{X}_A = (X_{i_1}, \dots, X_{i_m})$  which takes values  $\mathbf{X}_A = \mathbf{x}_A = (x_{i_1}, \dots, x_{i_m}) \in \mathcal{X}_A = \mathcal{X}_{i_1} \times \dots \times \mathcal{X}_{i_m}$  and its marginal is denoted by  $Q_A$ . The conditional probability distribution of  $X_i$  given parents values  $\mathbf{X}_{\text{Pa}(i)} = \mathbf{x}_{\text{Pa}(i)}$  is denoted by  $Q_{i|\text{Pa}(i)}$ , i.e.,  $Q_{i|\text{Pa}(i)}(dx_i) = Q(dx_i | \mathbf{X}_{\text{Pa}(i)} = \mathbf{x}_{\text{Pa}(i)})$  with corresponding density  $q(x_i | \mathbf{x}_{\text{Pa}(i)})$ . In general, for two sets of indices  $A, B \subset V$ ,  $Q_{A|B}(d\mathbf{x}_A) = Q(d\mathbf{x}_A | \mathbf{X}_B = \mathbf{x}_B)$ . Having all notation and terminology in place, we next define Bayesian networks formally.

**Definition 4.1** (Bayesian network over a DAG). A Bayesian network over a DAG  $G = (V, E)$  with variables  $X_i \in \mathcal{X}_i$  is the pair  $(G, Q)$  such that the joint probability distribution  $Q$  factorizes as

$$Q(dx_1, \dots, dx_n) = \prod_{i=1}^n Q_{i|\text{Pa}(i)}(dx_i | \mathbf{X}_{\text{Pa}(i)} = \mathbf{x}_{\text{Pa}(i)}),$$

with  $\text{Pa}(i)$  the parent set (and  $Q_{i|\text{Pa}(i)}$  the CPDs, or marginals if  $\text{Pa}(i) = \emptyset$ ).

For any set  $A \subset V$ , we denote  $A^c = V \setminus A$ . The set of probability distributions that factorize according to  $G$  with vertex set  $V = \{1, \dots, n\}$  and edge set  $E \subset V \times V$  is denoted by  $\mathcal{P}^G$ . Given a Bayesian network  $(G, Q)$ , the marginal distribution  $Q_A$  of  $\mathbf{X}_A$  has the form

$$Q_A(d\mathbf{x}_A) = \int_{\mathcal{X}_{\rho_A}} \prod_{i \in A} Q_{i|\text{Pa}(i)}(dx_i) \prod_{j \in \rho_A} Q_{j|\text{Pa}(j)}(dx_j)$$

where  $\rho_A$  is the set of indices of all the ancestors of  $A$  with respect to graph  $G$ .

We now fix  $Q \in \mathcal{P}^G$ . For each vertex  $i \in V$ , we define the following spaces of probability distributions:

$$\mathcal{P}_i^G = \left\{ Q_{V^{(i-1)}|\text{Pa}(i)} \otimes P_{i \cup \text{Pa}(i)} \otimes \prod_{j=i+1}^n Q_{j|\text{Pa}(j)} : P_{i \cup \text{Pa}(i)} \in \mathcal{P}(\mathcal{X}_{i \cup \text{Pa}(i)}) \right\} \quad (8)$$

where  $V^{(i)} = \{1, \dots, i\} \setminus \text{Pa}(i+1)$  with  $i = 1, \dots, n-1$ , and the symbol  $\otimes$  between probability distributions means the product of distributions, i.e., if  $\mu_1, \dots, \mu_n$  are probability distributions on  $\mathcal{X}_1, \dots, \mathcal{X}_n$ , respectively, then

$$\mu_1 \otimes \dots \otimes \mu_n(d\mathbf{x}) = \mu_1(dx_1) \dots \mu_n(dx_n).$$

The probability space given in (8) maintains the graph-structure of  $G$ . For  $\gamma \in \Gamma$ , we introduce the conditional  $Q$ -expectation operators as follows:

$$I_{i, \text{Pa}(i)}[\gamma](x_i, \mathbf{x}_{\text{Pa}(i)}) = \int_{\mathcal{X}_{V^{(i-1)}}} \int_{\mathcal{X}_{i+1}} \cdots \int_{\mathcal{X}_n} \gamma(\mathbf{x}) \prod_{j=i+1}^n Q_{j|\text{Pa}(j)}(dx_j) Q_{V^{(i-1)}|\text{Pa}(i)}(d\mathbf{x}_{V^{(i-1)}}). \quad (9)$$

Moreover, for each vertex  $i \in V$ , we define the following sets:

$$I_{i, \text{Pa}(i)}[\Gamma] = \{I_{i, \text{Pa}(i)}[\gamma] : \gamma \in \Gamma\}$$

and  $\Gamma_{i \cup \text{Pa}(i)}$  is the same function space  $\Gamma$  restricted to the subspace  $\mathcal{X}_{i \cup \text{Pa}(i)}$ . For example, if  $\Gamma = \text{Lip}_b^1(\mathcal{X})$ , then  $\Gamma_{i \cup \text{Pa}(i)} = \text{Lip}_b^1(\mathcal{X}_{i \cup \text{Pa}(i)})$ .

The operators  $I_{i, \text{Pa}(i)}$  and the associated projected classes  $I_{i, \text{Pa}(i)}[\Gamma]$  provide the mechanism by which a global discriminator objective on  $\mathcal{X}$  can be averaged over the conditional structure of  $Q$  and restricted to the local family  $i \cup \text{Pa}(i)$ . They therefore form the bridge between the general variational discrepancies introduced in Section 3.1 and the graph-structured objectives studied next. We now use this notation to show how global discrepancy minimization over  $\mathcal{P}^G$  can, under suitable conditions, be related to collections of local family-level problems.

## 5 GRAPH-INFORMED GANS

In this section, we combine the variational discrepancy framework of Section 3 with the Bayesian-network operators introduced in Section 4. We show that the global discrepancy minimization can be replaced by a principled surrogate, a minimization over family-level objectives on the neighborhoods  $i \cup \text{Pa}(i)$ . We first recall generalized subadditivity from Ding et al. (2021), then introduce an infimal version suited to interpolative divergences, and finally state our main results for  $(f, \Gamma)$ -divergences, IPMs, and proximal optimal transport divergences. These results provide the theoretical basis for graph-informed GANs.

In Ding et al. (2021), the authors establish generalized subadditivity bounds for a broad class of probability distances and divergences, including the Jensen–Shannon divergence, the Wasserstein distance, and nearly all  $f$ -divergences. We reproduce these key bounds in Definition 5.1 below for the convenience of the reader. Throughout the remainder of this section, we fix a graph structure  $G$  and recall that  $\mathcal{P}^G$  denotes the class of probability distributions that factorize according to  $G$ .

**Definition 5.1** (Generalized subadditivity (Ding et al., 2021)). Let  $P, Q \in \mathcal{P}^G$  be a Bayesian network with underlying graph  $G$ . Given measures of discrepancy  $\delta$  and  $\delta'$ , we say that  $\delta$  satisfies  $\alpha$ -linear *generalized subadditivity with error  $\epsilon$*  with respect to  $\delta'$  on Bayesian networks if, for all such  $P, Q$ , the following inequality holds:

$$\delta'(Q, P) - \epsilon \leq \alpha \sum_{i=1}^n \delta(Q_{i \cup \text{Pa}(i)}, P_{i \cup \text{Pa}(i)}).$$

For the case  $\delta = \delta'$ ,  $\epsilon = 0$  and  $\alpha = 1$  we say that  $\delta$  satisfies subadditivity on Bayesian networks.

By contrast, interpolative divergences presented in Section 3.4—which have demonstrated strong empirical performance in generative modeling—have not been systematically studied from a subadditivity perspective. One reason is that these divergences are typically defined through primal–dual (variational) formulations (see (5) and (4)), rather than through the classical representation (2). Moreover, the absence of a triangle inequality from divergences does not help in establishing the subadditivity bound, see e.g., Theorem 6 and its proof in Ding et al. (2021). These considerations introduce technical challenges that require different handling. Before introducing our new infimal notion, we record a simple consequence of existing subadditivity results together with the primal representation of  $(f, \Gamma)$ -divergences. This provides a useful benchmark but also illustrates that the resulting bounds are not yet in the form required for our later graph-local variational analysis.

**Theorem 5.2.** *If  $(\mathcal{X}, d)$  is a finite metric space, the  $(f_{\text{KL}}, \text{Lip}_b^L(\mathcal{X}))$ -divergence, for any  $L > 0$ , satisfies  $\left(\frac{2 \text{diam}(\mathcal{X})}{d_{\min}}\right)$ -linear subadditivity on Bayesian networks, where  $\text{diam}(\mathcal{X}) = \max_{\mathbf{x}, \mathbf{y} \in \mathcal{X}} d(\mathbf{x}, \mathbf{y})$  and  $d_{\min} = \min_{\substack{\mathbf{x}, \mathbf{y} \in \mathcal{X} \\ \mathbf{x} \neq \mathbf{y}}} d(\mathbf{x}, \mathbf{y})$ .*

*Proof.* By using the primal formulation of  $(f, \Gamma)$ -divergences given in (5), the subadditivity of KL-divergence and 1-Wasserstein given in Theorem 3 and Corollary 7 in Ding et al. (2021) and the fact that

$$\mathfrak{D}_f^{\Gamma^L}(Q\|P) = \inf_{R \in \mathcal{P}(\mathcal{X})} \{LW_1(Q, R) + \mathfrak{D}_{f_{\text{KL}}}(R\|P)\} \leq \inf_{R \in \mathcal{P}^G} \{LW_1(Q, R) + \mathfrak{D}_{f_{\text{KL}}}(R\|P)\}$$

the result follows.  $\square$

### 5.1 INFIMAL SUBADDITIVITY FOR BAYESIAN NETWORKS OVER A DAG

Although Ding et al. (2021) proves subadditivity for  $f$ -divergences in a restricted setting where the distributions  $P$  and  $Q$  are sufficiently close, this framework does not directly cover interpolative divergences such as  $(f, \Gamma)$ -divergences. The difficulty is that interpolative divergences are defined via infimal convolution and variational representations rather than via the classical density-based form of  $f$ -divergences. This suggests replacing classical subadditivity by a weaker notion that is tailored to optimization over structured model classes. Motivated by this gap, we introduce  $\alpha$ -linear generalized infimal subadditivity and additivity on Bayesian networks, formalized in the next definition.

**Definition 5.3.** Let  $Q \in \mathcal{P}^G$  be a Bayesian network with underlying graph  $G$ . Given measures of discrepancy  $\delta, \delta_1, \dots, \delta_n$ , we say that  $\delta$  satisfies  $\alpha$ -linear generalized infimal subadditivity with respect to  $\delta_1, \dots, \delta_n$  on Bayesian networks if, for all such  $Q$ , the following inequality holds:

$$\inf_{P \in \mathcal{P}(\mathcal{X})} \delta(Q, P) \leq \inf_{P \in \mathcal{P}(\mathcal{X})} \alpha \sum_{i=1}^n \delta_i(Q_{i \cup \text{Pa}(i)}, P_{i \cup \text{Pa}(i)}). \quad (10)$$

For the case  $\delta = \delta_1 = \dots = \delta_n$ , we say that  $\delta$  satisfies infimal subadditivity on Bayesian networks. Furthermore we say that  $\delta$  satisfies  $\alpha$ -linear generalized infimal additivity with respect to  $\delta_1, \dots, \delta_n$  on Bayesian networks if (10) holds with equality.

Although the optimization problem in (10) may be viewed as graph-constrained in spirit, the infima are taken over all  $P \in \mathcal{P}(\mathcal{X})$ . This is important for applications as even when the target  $Q$  factorizes according to  $G$ , it is generally difficult to enforce the same structural constraint on the optimizer  $P^*$  during training. The usefulness of infimal subadditivity is therefore that it replaces a difficult global optimization problem by a surrogate built from family-level discrepancies, without requiring the optimizer itself to be explicitly parameterized as an element of  $\mathcal{P}^G$ .

We now show that this principle applies to the main discrepancy classes considered in this paper. Under suitable assumptions,  $(f, \Gamma)$ -divergences,  $\Gamma$ -IPMs, and proximal optimal transport divergences all admit graph-informed upper bounds in terms of local family objectives, and in the additive regime, these bounds become exact. We begin with the interpolative case  $(f, \Gamma)$ , which provides the basic template for the later results.

**Theorem 5.4.** Let  $G$  be an arbitrary DAG and  $L, L_1, \dots, L_n > 0$ . Suppose that  $I_{i, \text{Pa}(i)}[\Gamma^L] \subset \Gamma_{i \cup \text{Pa}(i)}^{L_i}$  for all  $i \in V$ . Then,  $(f, \Gamma)$ -divergences satisfy  $\frac{1}{n}$ -linear generalized infimal subadditivity given in (10) with

$$\delta = \mathfrak{D}_f^{\Gamma^L} \quad \text{and} \quad \delta_i = \mathfrak{D}_f^{\Gamma_{i \cup \text{Pa}(i)}^{L_i}} \quad \text{for all } i \in V.$$

Moreover, if  $L_i \leq L$  for all  $i \in V$ , then  $(f, \Gamma)$ -divergences satisfy  $\frac{1}{n}$ -linear generalized infimal additivity with  $\delta = \mathfrak{D}_f^{\Gamma^L}$  and  $\delta_i = \mathfrak{D}_f^{\Gamma_{i \cup \text{Pa}(i)}^{L_i}}$  for all  $i \in V$ .

*Proof.* The proof of the theorem relies on a sequence of data-processing-type inequalities involving the operators  $I_{i, \text{Pa}(i)}$ , together with the corresponding assumptions  $I_{i, \text{Pa}(i)}[\Gamma^L] \subset \Gamma_{i \cup \text{Pa}(i)}^{L_i}$  for all  $i \in V$ . To clarify the main ideas and highlight the role played by these operators, we first present the proof for the simple DAG

$$X_1 \longrightarrow X_2 \longrightarrow X_3, \quad (11)$$

while the proof for a Bayesian network defined on an arbitrary DAG comes next. Let  $\gamma \in \Gamma^L$ , we begin with computing the expectation of  $I_{1,2}[\gamma]$  with respect to  $Q_{\{1,2\}}$ . A direct calculation gives us

$$E_{Q_{\{1,2\}}} [I_{1,2}[\gamma]] = \int_{\mathcal{X}_1} \int_{\mathcal{X}_2} \int_{\mathcal{X}_3} \gamma(x_1, x_2, x_3) Q_{\{1,2\}}(dx_1, dx_2) Q_{3|2}(dx_3) = E_Q[\gamma].$$

For  $P_{\{1,2\}} \in \mathcal{P}(\mathcal{X}_{\{1,2\}})$  (we remind that  $\mathcal{X}_{\{1,2\}} = \mathcal{X}_1 \times \mathcal{X}_2$ ), for any function  $f$  as defined in Section 3.1 and for  $\nu \in \mathbb{R}$ , the convexity  $f^*$ , Jensen's inequality, and (9) give:

$$E_{P_{\{1,2\}}} [f^*(I_{1,2}[\gamma] - \nu)] \leq E_{P_{\{1,2\}}} [I_{1,2}[f^*(\gamma - \nu)]] = E_{P_{\{1,2\}} \otimes Q_{3|2}} [f^*(\gamma - \nu)].$$

where  $P_{\{1,2\}} \otimes Q_{3|2} \in \mathcal{P}_2^G$  is defined in (8).

Subtracting (13) from (12) and taking the infimum over  $\nu \in \mathbb{R}$  on both sides yields, for all  $\gamma \in \Gamma^L$ ,

$$\begin{aligned} E_{Q_{\{1,2\}}} [I_{1,2}[\gamma]] - \inf_{\nu \in \mathbb{R}} \{ \nu + E_{P_{\{1,2\}}} [f^*(I_{1,2}[\gamma - \nu])] \} \\ \geq E_Q[\gamma] - \inf_{\nu \in \mathbb{R}} \{ \nu + E_{P_{\{1,2\}} \otimes Q_{3|2}} [f^*(\gamma - \nu)] \}. \end{aligned}$$

Then taking the supremum over  $\gamma \in \Gamma^L$  in both sides of the inequality above, we obtain

$$\mathfrak{D}_f^{I_{1,2}[\Gamma^L]}(Q_{\{1,2\}} \| P_{\{1,2\}}) \geq \mathfrak{D}_f^{\Gamma^L}(Q \| P_{\{1,2\}} \otimes Q_{3|2}), \quad (14)$$

by definition in (4). We similarly obtain

$$\mathfrak{D}_f^{I_1[\Gamma^L]}(Q_{\{1\}} \| P_{\{1\}}) \geq \mathfrak{D}_f^{\Gamma^L}(Q \| P_{\{1\}} \otimes Q_{3|2} \otimes Q_{2|1}),$$

and

$$\mathfrak{D}_f^{I_{2,3}[\Gamma^L]}(Q_{\{2,3\}} \| P_{\{2,3\}}) \geq \mathfrak{D}_f^{\Gamma^L}(Q \| P_{\{2,3\}} \otimes Q_{1|2}).$$

We define

$$c = \inf_{P \in \mathcal{P}(\mathcal{X})} \mathfrak{D}_f^{\Gamma^L}(Q \| P);$$

since  $\mathcal{P}_i^G \subset \mathcal{P}^G \subset \mathcal{P}(\mathcal{X})$ , in particular it holds that

$$\mathfrak{D}_f^{I_1[\Gamma^L]}(Q_{\{1\}} \| P_{\{1\}}) + \mathfrak{D}_f^{I_{1,2}[\Gamma^L]}(Q_{\{1,2\}} \| P_{\{1,2\}}) + \mathfrak{D}_f^{I_{2,3}[\Gamma^L]}(Q_{\{2,3\}} \| P_{\{2,3\}}) \geq 3c. \quad (15)$$

Then we consider infimum over  $P \in \mathcal{P}^G$  on both sides yields (10). Furthermore, from (14)–(15) and the fact that  $I_{i, \text{Pa}(i)}[\Gamma^L] \subset \Gamma^{L_i}$  for all  $i \in V$ , we obtain

$$\mathfrak{D}_f^{\Gamma^{L_1}}(Q \| P_{\{1\}} \otimes Q_{3|2} \otimes Q_{2|1}) + \mathfrak{D}_f^{\Gamma^{L_2}}(Q \| P_{\{1,2\}} \otimes Q_{3|2}) + \mathfrak{D}_f^{\Gamma^{L_3}}(Q \| P_{\{2,3\}} \otimes Q_{1|2}) \geq 3c.$$

For the other direction, it is enough to observe that when  $I_{i, \text{Pa}(i)}[\Gamma] \subset \Gamma^{L_i}$  for all  $i \in V$

$$\mathfrak{D}_f^{I_{i, \text{Pa}(i)}[\Gamma^L]}(Q_{i \cup \text{Pa}(i)} \| P_{i \cup \text{Pa}(i)}) \leq \mathfrak{D}_f^{\Gamma^{L_i}}(Q_{i \cup \text{Pa}(i)} \| P_{i \cup \text{Pa}(i)}) \leq \mathfrak{D}_f^{\Gamma^L}(Q \| P), \quad (16)$$

where the last inequality comes from the fact that  $L_i \leq L$  for all  $i \in V$ . Then the strict additivity follows.

For a general DAG  $G$ , it suffices to observe that for any  $i \in V$

$$E_{P_{i \cup \text{Pa}(i)}} [I_{i, \text{Pa}(i)}[\gamma]] = \int_{\mathcal{X}} \gamma(\mathbf{x}) \tilde{P}(d\mathbf{x}) = E_{\tilde{P}}[\gamma]$$

where  $\tilde{P} = Q_{V(i) \setminus i \cup \text{Pa}(i)} \otimes P_{i \cup \text{Pa}(i)} \otimes \prod_{j=i+1}^n Q_{j|\text{Pa}(j)} \in \mathcal{P}_i^G$  and

$$E_{Q_{i \cup \text{Pa}(i)}} [f^*(I_{i, \text{Pa}(i)}[\gamma] - \nu)] \leq E_Q [f^*(\gamma - \nu)].$$

The other direction given in (16) remains unchanged, and combining both inequalities completes the proof.  $\square$

*Remark 5.5.* In Theorem 5.4, the infimum can also be taken over  $P \in \mathcal{P}^G$ ; this follows directly from the proof. In practice, however, enforcing the graph structure directly in the generator class is challenging. For this reason, we retain the larger space  $\mathcal{P}(\mathcal{X})$ .

Theorem 5.4 gives a variational justification for replacing a monolithic discriminator acting on the full joint space with a graph-informed collection of family-level discriminators aligned with  $G$ . In practice, if the generator is restricted to  $P_\theta \in \mathcal{P}(\mathcal{X})$ , one may train by minimizing the graph-informed surrogate

$$\mathcal{L}_{\text{loc}}(\theta) = \frac{1}{n} \sum_{i=1}^n \sup_{\gamma_i \in \Gamma_{i \cup \text{Pa}(i)}^{L_i}} \{ E_Q[\gamma_i(\mathbf{x}_{i \cup \text{Pa}(i)})] - \inf_{\nu \in \mathbb{R}} (\nu + E_{P_\theta} [f^*(\gamma_i(\mathbf{x}_{i \cup \text{Pa}(i)}) - \nu)]) \}. \quad (17)$$

Thus the attained value of  $\mathcal{L}_{\text{loc}}(\theta)$  provides an explicit upper bound (certificate) on the best achievable global interpolative divergence within  $\mathcal{P}(\mathcal{X})$ . In the additive regime, minimizing  $\mathcal{L}_{\text{loc}}$  is equivalent to minimizing the corresponding global objective.

To illustrate the meaning of Theorem 5.4 before turning to the corresponding IPM and proximal optimal transport results, we consider an application to a synthetic data set in which the graph structure is known. The purpose of this example is twofold: first, to assess whether the graph-informed surrogate tracks the best achievable global objective, and second, to test whether graph alignment improves recovery of the underlying conditional structure.

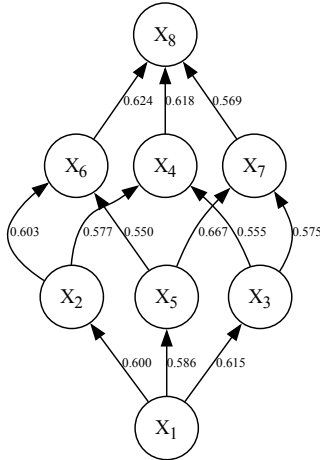


Figure 1: The linear-Gaussian Bayesian network given by the Hasse diagram of the subset lattice for the 8 subsets of a three-element set. The edge weights from node  $j$  to  $i$  are the parent coefficients  $\phi_{ji} \sim N(\mu_\phi = 0.6, \sigma_\phi^2 = 0.05^2)$  in (18), which are fixed once across all experiments.

We consider a linear-Gaussian Bayesian network on eight variables, shown in Figure 1, defined by

$$X_i = \sum_{j \in \text{Pa}(i)} \phi_{ji} X_j + \epsilon_i, \quad i \in \{1, \dots, 8\}, \tag{18}$$

where  $\epsilon_i \sim N(0, \sigma^2)$  with  $\sigma = 0.5$  and the root node satisfies  $X_1 \sim N(0, 1)$ . This model provides a direct testbed for Theorem 5.4, since the correct family structure is known through the parent coefficients  $\{\phi_{ji}\}$  (full details of the experiment can be found in Section 6).

Figure 2a compares a graph-agnostic GAN, whose monolithic discriminator acts on the full joint distribution, with a graph-informed GAN built from family-level discriminator classes on  $\{i \cup \text{Pa}(i)\}_{i=1}^8$ . We report both the classical setting, based on unrestricted  $f$ -divergence objectives, and the interpolative setting, based on constrained  $(f, \Gamma)$ -divergence objectives when  $f = f_{\text{KL}}$  and  $\Gamma = \text{Lip}_b$ . In the interpolative setting, the graph-informed surrogate closely tracks the best achieved global objective and exhibits substantially lower variability across seeds. By contrast, in the classical setting the graph-agnostic objective is markedly more variable, reflecting the greater difficulty of the full-joint discrimination problem.

To connect objective values with the structural fidelity of model predictions, Figure 2b reports recovery of the parent coefficients  $\{\phi_{ji}\}$  from generated samples for the experiments based on the interpolative divergences. We also include a misaligned multi-discriminator baseline with matched family sizes but randomly assigned parent sets. The graph-informed approach achieves lower estimation error and smaller variability than both the graph-agnostic and misaligned multi-discriminator baselines. This is consistent with the interpretation of Theorem 5.4, that when the local discriminator classes are matched to the true graph structure, they control precisely the family-level distributions needed to recover the conditional relationships.

Taken together, these diagnostics show that the graph-informed surrogate is not only theoretically justified but also practically meaningful: in the interpolative regime it provides a stable proxy for the global objective, while preserving the structural information encoded by the Bayesian network. We now return to the theory and state the analogous result for  $\Gamma$ -IPMs.

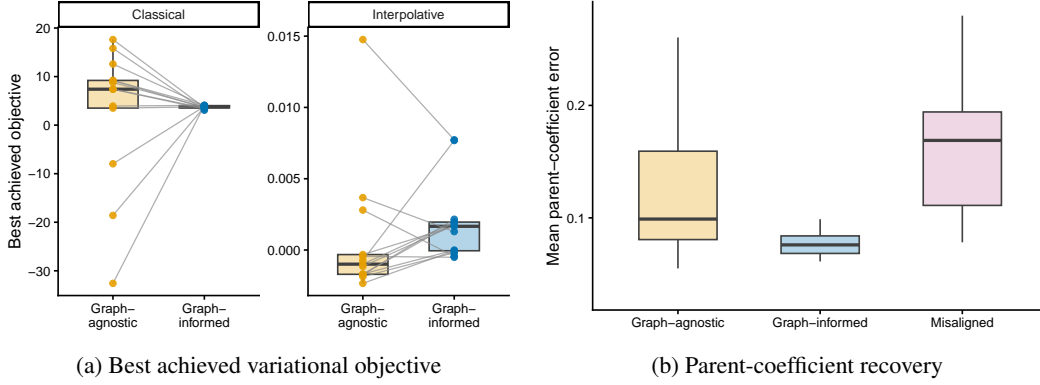


Figure 2: Objective-level and structural diagnostics for the structured linear-Gaussian model (18) under graph-agnostic and graph-informed adversarial training; see Figure 1 for the underlying Hasse network. (a) Best achieved validation variational objective, i.e., the minimum variational loss attained over training epochs for the validation set. Values closer to zero indicate a closer fit, and gray line segments pair runs with the same random seed. In the interpolative setting, the graph-informed multi-discriminator surrogate attains values close to those of the graph-agnostic monolithic objective, consistent with the interpretation of Theorem 5.4. (b) Mean  $L_2$  error in the recovered parent coefficients, averaged over non-root nodes, with lower values indicating better recovery of the underlying conditional structure. Here, the graph-informed construction aligned with the true families outperforms both the graph-agnostic baseline and the misaligned multi-discriminator construction. Boxplots summarize 13 paired runs per model.

**Theorem 5.6.** *Let  $G$  be an arbitrary DAG and  $L, L_1, \dots, L_n > 0$ . Suppose that  $I_{i, \text{Pa}(i)}[\Gamma^L] \subset \Gamma_{i \cup \text{Pa}(i)}^{L_i}$  for all  $i \in V$ . Then, IPMs satisfy  $\frac{1}{n}$ -linear generalized infimal subadditivity given in (10) with*

$$\delta = W^{\Gamma^L} \quad \text{and} \quad \delta_i = W^{\Gamma_{i \cup \text{Pa}(i)}^{L_i}} \quad \text{for all } i \in V.$$

*Moreover, if  $L_i \leq L$  for all  $i \in V$ , then IPMs satisfy  $\frac{1}{n}$ -linear generalized infimal additivity with the same  $\delta$  and  $\delta_i$  as above.*

*Proof.* The proof follows the same arguments as that of Theorem 5.4 and is therefore omitted.  $\square$

The same principle extends beyond variational divergences and  $\Gamma$ -IPMs to transport-based discrepancies. We next show that proximal optimal transport divergences also admit an infimal subadditivity structure over Bayesian-network families.

**Theorem 5.7.** *Let  $c$  be any cost function on  $\mathcal{X}$ . Then, proximal optimal transport divergences satisfy  $\frac{1}{n}$ -linear generalized infimal subadditivity given in (10) with*

$$\delta = \mathfrak{D}_{\text{KL}, \varepsilon}^c \quad \text{and} \quad \delta_i = \mathfrak{D}_{\text{KL}, \varepsilon}^{c_i} \quad \text{for all } i \in V,$$

where

$$c_i(\mathbf{x}_{i \cup \text{Pa}(i)}, \mathbf{x}'_{i \cup \text{Pa}(i)}) = \int_{\mathcal{X}_{[i \cup \text{Pa}(i)]^c}} \int_{\mathcal{X}_{[i \cup \text{Pa}(i)]^c}} c(\mathbf{x}, \mathbf{x}') Q^{(i)}(d\mathbf{x}_{[i \cup \text{Pa}(i)]^c}) Q^{(i)}(d\mathbf{x}'_{[i \cup \text{Pa}(i)]^c}),$$

where  $Q^{(i)} = Q_{V^{(i-1)} | \text{Pa}(i)} \otimes \prod_{j=i+1}^n Q_{j | \text{Pa}(j)}$  is the marginal distribution of  $\mathbf{X}_{[i \cup \text{Pa}(i)]^c}$ . Moreover, the proximal optimal transport divergences made by  $c(\mathbf{x}, \mathbf{y}) = \|\mathbf{x} - \mathbf{y}\|_p^p = \sum_{i=1}^n \|x_i - y_i\|_p^p$  (i.e.,  $p$ -Wasserstein distance) and KL-divergence, satisfy  $\frac{1}{n}$ -infimal additivity with  $\delta_i = \mathfrak{D}_{\text{KL}, \varepsilon}^{c_i}$  with  $c_i(x_i, y_i) = \|x_i - y_i\|_p^p$ , for all  $i \in V$ .

*Proof.* Following the same strategy as in Theorem 5.4, for the simple DAG (11) we obtain

$$\begin{aligned} & \sup_{\phi \oplus \psi \leq c} \left\{ \mathbb{E}_Q[\phi] - \varepsilon \ln \mathbb{E}_{P_{\{1,2\}} \otimes Q_{3|2}}[e^{-\psi/\varepsilon}] \right\} \\ & \leq \sup_{\phi \oplus \psi \leq c} \left\{ \mathbb{E}_{Q_{\{1,2\}}}[I_{1,2}[\phi]] - \varepsilon \ln \mathbb{E}_{P_{\{1,2\}}}[e^{-I_{1,2}[\psi]/\varepsilon}] \right\} \\ & \leq \sup_{\tilde{\phi} \oplus \tilde{\psi} \leq c_2} \left\{ \mathbb{E}_{Q_{\{1,2\}}}[\tilde{\phi}] - \varepsilon \ln \mathbb{E}_{P_{\{1,2\}}}[e^{-\tilde{\psi}/\varepsilon}] \right\} \end{aligned}$$

where the second inequality comes from the fact that

$$\begin{aligned} I_{1,2}[\phi](x_1, x_2) + I_{1,2}[\psi](x'_1, x'_2) &= \int_{\mathcal{X}_3} \phi(x_1, x_2, x_3) Q_{3|2}(dx_3) + \int_{\mathcal{X}_3} \psi(x'_1, x'_2, x'_3) Q_{3|2}(dx'_3) \\ &= \int_{\mathcal{X}_3} \int_{\mathcal{X}_3} (\phi(x_1, x_2, x_3) + \psi(x'_1, x'_2, x'_3)) Q_{3|2}(dx_3) Q_{3|2}(dx'_3) \\ &\leq \int_{\mathcal{X}_3} \int_{\mathcal{X}_3} c(\mathbf{x}, \mathbf{x}') Q_{3|2}(dx_3) Q_{3|2}(dx'_3) \end{aligned}$$

Then, the result follows as in proof of Theorem 5.4. The proof of the second part of the theorem is based on Theorem 3.7 in Baptista et al. (2025). Specifically,

$$\begin{aligned} \mathfrak{D}_{\text{KL},\varepsilon}^p(Q\|P) &= \mathfrak{D}_{\text{KL},\varepsilon}^p(Q_{\{1,2\}} \otimes Q_{3|2} \| P_{\{1,2\}} \otimes Q_{3|2}) \\ &\leq \inf_{R_{\{1,2\}} \otimes R_{3|2}} \inf_{\substack{\pi \in \Pi(Q_{\{1,2\}}, R_{\{1,2\}}), \\ \tilde{\pi} \in \Pi(Q_{3|2}, R_{3|2})}} \left\{ \int \|\mathbf{x}_{\{1,2\}} - \mathbf{y}_{\{1,2\}}\|_p^p d\pi + \varepsilon \mathfrak{D}_{\text{KL}}(R_{\{1,2\}} \| P_{\{1,2\}}) \right. \\ &\quad \left. + \int \|x_3 - y_3\|_p^p d\tilde{\pi} + \varepsilon \mathfrak{D}_{\text{KL}}(R_{3|2} \| Q_{3|2}) \right\} \\ &\leq \mathfrak{D}_{\text{KL},\varepsilon}^p(Q_{\{1,2\}} \| P_{\{1,2\}}) + \mathfrak{D}_{\text{KL},\varepsilon}^p(Q_{3|2} \| Q_{3|2}) = \mathfrak{D}_{\text{KL},\varepsilon}^p(Q_{\{1,2\}} \| P_{\{1,2\}}) \end{aligned}$$

For the other direction, we work exactly the same as in the proof of Theorem 3.7 in Baptista et al. (2025). Based on the above, one can generalize to any DAG, similar to the proof of Theorem 5.4.  $\square$

From the perspective of adversarial learning, the preceding theorems justify replacing a graph-agnostic GAN with a monolithic discriminator by a graph-informed GAN with family-level discriminators. This is not only a computational simplification; since GAN training amounts to a learned two-sample testing problem (Goodfellow et al., 2014; Nowozin et al., 2016), localization decomposes a high-dimensional discrimination task into a collection of lower-dimensional subproblems that are easier to optimize and diagnose. Theorems 5.4, 5.6, and 5.7 show that these local games define principled surrogates for the corresponding graph-constrained global objectives.

In Section 5.2, we provide examples and discuss conditions under which the condition in Theorem 5.4 which we henceforth denote by

$$(C) \quad I_{i, \text{Pa}(i)}[\Gamma^L] \subset \Gamma_{i \cup \text{Pa}(i)}^{L_i} \quad \text{for all } i \in V,$$

holds, as well as its interpretation from the perspective of generative modeling. When the condition (C) is violated, we can still obtain meaningful lower and upper bounds for  $(f, \Gamma)$ -divergences and IPMs. Specifically, for any  $P, Q \in \mathcal{P}^G$ , we have the following lower bound:

$$\frac{1}{n} \sum_{i=1}^n \mathfrak{D}_f^{\Gamma_{i \cup \text{Pa}(i)}^{L_i}}(Q_{i \cup \text{Pa}(i)} \| P_{i \cup \text{Pa}(i)}) \leq \mathfrak{D}_f^{\Gamma^L}(Q\|P)$$

and for any  $Q \in \mathcal{P}^G$ , we obtain

$$\inf_{P \in \mathcal{P}(\mathcal{X})} \mathfrak{D}_f^{\Gamma^L}(Q\|P) \leq \inf_{P \in \mathcal{P}(\mathcal{X})} \frac{1}{n} \sum_{i=1}^n \mathfrak{D}_f^{I_{i, \text{Pa}(i)}[\Gamma^L]}(Q_{i \cup \text{Pa}(i)} \| P_{i \cup \text{Pa}(i)}).$$

The same lower and upper bounds hold for IPMs. This follows directly from the monotonicity property  $\mathfrak{D}_f^{\Gamma_{i \cup \text{Pa}(i)}}(Q_{i \cup \text{Pa}(i)} \| P_{i \cup \text{Pa}(i)}) \leq \mathfrak{D}_f^{\Gamma}(Q\|P)$  for all  $i \in V$ . The proof of the upper bound is already contained in the proof of Theorem 5.4. Next, we state a lemma that provides sufficient conditions for subadditivity of a function and will be used in Remark 5.9 and Example 5.10.

**Lemma 5.8.** *If  $F : [0, \infty) \rightarrow \mathbb{R}$  is concave and  $F(0) = 0$  (or more general  $F(0) \geq 0$ ), then  $F$  satisfies sub-additivity, i.e.  $F(x + y) \leq F(x) + F(y)$  for every  $x, y \in [0, \infty)$ .*

*Proof.* It is enough to observe that

$$\begin{aligned} F(x) &= F\left(\frac{y}{x+y} \cdot 0 + \frac{x}{x+y}(x+y)\right) \geq \frac{x}{x+y} F(x+y) \\ F(y) &= F\left(\frac{x}{x+y} \cdot 0 + \frac{y}{x+y}(x+y)\right) \geq \frac{y}{x+y} F(x+y) \end{aligned}$$

By summing the above inequalities, we obtain sub-additivity, i.e.,

$$F(x) + F(y) \geq \frac{x}{x+y} F(x+y) + \frac{y}{x+y} F(x+y) = F(x+y)$$

□

*Remark 5.9* (Graph-informed  $\Gamma$ ). A special case where the discriminator class is explicitly aligned with the graph structure, as each component depends only on a node and its parent set is given by

$$\Gamma = \bigoplus_{i=1}^n \Gamma_{i \cup \text{Pa}(i)} = \left\{ \sum_{i=1}^n \gamma_i(x_i, \mathbf{x}_{\text{Pa}(i)}) : \gamma_i \in \Gamma_{i \cup \text{Pa}(i)} \text{ for all } i \in V \right\}.$$

Each element of the discriminator space decomposes additively over local neighborhoods, which makes the subadditivity property for IPMs immediate:

$$W^{\bigoplus_{i=1}^n \Gamma_{i \cup \text{Pa}(i)}}(Q_{i \cup \text{Pa}(i)} \| P_{i \cup \text{Pa}(i)}) \leq \sum_{i=1}^n W^{\Gamma_{i \cup \text{Pa}(i)}}(Q_{i \cup \text{Pa}(i)} \| P_{i \cup \text{Pa}(i)}).$$

Furthermore, since  $-f^*$  in the variational representation of the  $(f, \Gamma)$ -divergences is concave and satisfies  $-f^*(0) \geq 0$  (see Lemma 42 in Birrell et al. (2022a)), by Lemma 5.8, the following subadditivity property for  $(f, \Gamma)$ -divergences holds

$$\mathfrak{D}_f^{\bigoplus_{i=1}^n \Gamma_{i \cup \text{Pa}(i)}}(Q_{i \cup \text{Pa}(i)} \| P_{i \cup \text{Pa}(i)}) \leq \sum_{i=1}^n \mathfrak{D}_f^{\Gamma_{i \cup \text{Pa}(i)}}(Q_{i \cup \text{Pa}(i)} \| P_{i \cup \text{Pa}(i)}).$$

(i.e., using the fact that  $-f^*(\sum_{i=1}^n \gamma_i(x_i, \mathbf{x}_{\text{Pa}(i)})) \leq -\sum_{i=1}^n f^*(\gamma_i(x_i, \mathbf{x}_{\text{Pa}(i)}))$ ).

*Example 5.10* (Subadditivity for KL-divergence via variational representation). In Section 4.1 of Ding et al. (2021), the authors establish subadditivity (see Definition 5.1) of the KL divergence on Bayesian networks over an arbitrary DAG  $G$ , by relying on the definition (2). In contrast, in this example, we re-establish the subadditivity of the KL divergence on Bayesian networks using its variational characterization.

Precisely, let  $P, Q \in \mathcal{P}^G$ . Under appropriate assumptions (see Broniatowski and Keziou (2006)), the solution of (3) for  $f = f_{\text{KL}}$ , i.e.  $\mathfrak{D}_{\text{KL}}(Q \| P) = \sup_{\gamma \in \mathcal{M}_b(\mathcal{X})} \{E_Q[\gamma] - E_P[e^{\gamma-1}]\}$  is given by  $\gamma^* = \log\left(\frac{dQ}{dP}\right)$ . By the factorization of  $P$  and  $Q$  and it is straightforward to check that  $\gamma^* \in \bar{\Gamma} = \bigoplus_{i=1}^n \mathcal{M}_b(\mathcal{X}_{i \cup \text{Pa}(i)})$  because

$$\gamma^* = \sum_{i=1}^n \log \frac{Q_{i|\text{Pa}(i)}}{P_{i|\text{Pa}(i)}}, \quad Q\text{-a.s.}$$

Therefore,  $\mathfrak{D}_{\text{KL}}(Q \| P) = \mathfrak{D}_{\text{KL}}^{\bar{\Gamma}}(Q \| P)$ . We use Lemma 5.8 for  $f_{\text{KL}}^*$  and bound as follows:

$$\begin{aligned} \mathfrak{D}_{\text{KL}}^{\bar{\Gamma}}(Q \| P) &\leq \sup_{\substack{\bar{\gamma} = \sum_{i=1}^n h_i(x_i, \mathbf{x}_{\text{Pa}(i)}), \\ h_i \in \mathcal{M}_b(\mathcal{X}_{i \cup \text{Pa}(i)})}} \left\{ \sum_{i=1}^n E_Q[h_i] - E_P[e^{\sum_{i=1}^n h_i - 1}] \right\} \\ &\leq \sum_{i=1}^n \sup_{h_i \in \mathcal{M}_b(\mathcal{X}_{i \cup \text{Pa}(i)})} \{E_{Q_{i \cup \text{Pa}(i)}}[h_i] - E_{P_{i \cup \text{Pa}(i)}}[e^{h_i - 1}]\} \\ &\leq \sum_{i=1}^n \mathfrak{D}_{\text{KL}}(Q_{i \cup \text{Pa}(i)} \| P_{i \cup \text{Pa}(i)}) \end{aligned}$$

*Remark 5.11* (We cannot have subadditivity in general). The optimizer  $\gamma^*$  does not, in general, belong to the subspace  $\bar{\Gamma} \subset \Gamma$  which would be required to invoke subadditivity via concavity. As a result, one cannot directly apply Lemma 5.8, which leverages the concavity of  $-f^*$ , to establish the desired bound. In fact, let  $\mathbf{X} = (X_1, X_2, X_3)$  and  $R^*$  denote the optimal intermediate measure that solves (5). Indeed, by the properties of  $(f, \Gamma)$ -divergences and (6),

$$R^* \propto (f_{\text{KL}}^*)'(\gamma^*)dP = e^{\gamma^* - 1}dP$$

which together with the factorization of  $Q$ , we obtain

$$R^*(dx_1, dx_2, dx_3) = e^{\gamma^*(x_1, x_2, x_3) - 1} P_{3|2}(dx_3) P_{2|1}(dx_2) P_1(dx_1).$$

By explicitly computing the conditional distribution  $R_{3|\text{Pa}^{R^*}(3)}^*(dx_3)$ , where  $\text{Pa}^{R^*}(3)$  denotes the set of parents of node 3 under the distribution  $R^*$ , we obtain

$$R_{3|\text{Pa}^{R^*}(3)}^*(dx_3) = \frac{e^{\gamma^*(x_1, x_2, x_3) - 1} P_{3|2}(dx_3)}{E_{P_{3|2}}[e^{\gamma^* - 1}]}.$$

This expression reveals that  $\text{Pa}^{R^*}(3) = \{1, 2\} \neq \{2\} = \text{Pa}^Q(3)$ . Consequently, the optimal intermediate measure  $R^*$  does not share the same conditional independence structure as  $Q$ , which prevents the likelihood terms from being paired in the same manner as in (19).

*Remark 5.12* (Tighter bound). Although we have shown that the subadditivity-based upper bound for a Bayesian network depends explicitly on the underlying DAG  $G$  with  $n$  nodes—through the induced collection of local neighborhoods  $\{i \cup \text{Pa}(i)\}_{i=1}^n$ , which in turn determines the construction of the local discriminators—the choice of these neighborhoods is not unique. In particular, the local neighborhoods may be enlarged, leading to an alternative subadditivity-based upper bound that operates at a coarser level of granularity. Such bounds may typically be tighter, as they incorporate richer local dependencies. This flexibility arises because the proof of Theorem 5.4 hinges on establishing a data-processing-type inequality. Once this inequality is available, it allows the divergence to be further upper bounded by divergences between distributions defined on the remaining neighborhoods induced by the graph  $G$ . Consequently, the selection of local neighborhoods can be interpreted as an artificial hyperparameter that controls the trade-off between model complexity and tightness of the bound. In Child Bayesian network in Section 6.3, we illustrate this idea by replacing certain local neighborhoods with enlarged families that include additional ancestors.

The preceding results are abstract until condition (C) can be verified for concrete discriminator classes. We therefore next discuss representative choices of  $\Gamma$  for which the projection operators  $I_{i, \text{Pa}(i)}$  preserve the relevant function-space structure, thereby making the theory applicable in practice.

## 5.2 EXAMPLES OF ADMISSIBLE SETS SATISFYING CONDITION (C)

In this section, we provide examples of admissible sets that satisfy condition (C): bounded measurable functions and Lipschitz-bounded functions. These examples respectively recover the unrestricted  $f$ -divergence setting, and Wasserstein-type and Lipschitz-constrained discriminators.

**The space of bounded measurable functions  $\mathcal{M}_b(\mathcal{X})$ .** Let  $\Gamma = \mathcal{M}_b(\mathcal{X})$ . Then, for  $i \in V$ ,  $I_{i, \text{Pa}(i)}[\Gamma]$  is subset of the restricted version of  $\mathcal{M}_b(\mathcal{X})$  to  $\mathcal{X}_{i \cup \text{Pa}(i)}$ , i.e.,  $I_{i, \text{Pa}(i)}[\mathcal{M}_b(\mathcal{X})] \subset \mathcal{M}_b(\mathcal{X}_{i \cup \text{Pa}(i)})$ . In Theorem 11 of Ding et al. (2021), by assuming that  $P, Q$  are two-sided  $\epsilon$ -close (see Definition 2 in Ding et al. (2021)), they prove that any  $f$ -divergence whose  $f(\cdot)$  is continuous on  $(0, \infty)$  and twice differentiable at 1 with  $f''(1) > 0$  satisfies  $\alpha$ -linear subadditivity (see Definition 5.1). By applying Theorem 5.4, we prove that  $f$ -divergences satisfy  $\frac{1}{n}$ -linear infimal additivity.

**Theorem 5.13.** *Let  $G$  be an arbitrary DAG. Then,  $f$ -divergences satisfy  $\frac{1}{n}$ -linear generalized infimal additivity*

$$\inf_{P \in \mathcal{P}(\mathcal{X})} \mathfrak{D}_f(Q \| P) = \inf_{P \in \mathcal{P}(\mathcal{X})} \frac{1}{n} \sum_{i=1}^n \mathfrak{D}_f(Q_{i \cup \text{Pa}(i)} \| P_{i \cup \text{Pa}(i)})$$

*Proof.* It is enough to observe that

$$\mathfrak{D}_f^{\mathcal{M}_b(\mathcal{X}_{i \cup \text{Pa}(i)})}(Q_{i \cup \text{Pa}(i)} \| P_{i \cup \text{Pa}(i)}) = \mathfrak{D}_f(Q_{i \cup \text{Pa}(i)} \| P_{i \cup \text{Pa}(i)}).$$

□

**The space of Lipschitz bounded functions**  $\text{Lip}_b^L(\mathcal{X})$ ,  $L > 0$ . Suppose that  $\mathcal{X}$  is a metric space. The standard metric choice is

$$d(\mathbf{x}, \mathbf{x}') = \sum_{i=1}^n d_{\mathcal{X}_i}(x_i, x'_i),$$

for  $\mathbf{x} = (x_1, \dots, x_n)$  and  $\mathbf{x}' = (x'_1, \dots, x'_n)$ . Let  $\Gamma^L = \text{Lip}_b^L(\mathcal{X})$ . In this case, condition (C) can be satisfied if  $Q_{V^{(i)}|\text{Pa}(i)}(d\mathbf{x}_{V^{(i)}})$  with  $V^{(i)} = V \setminus [i \cup \text{Pa}(i)]$  viewed as a function of  $\mathbf{x}_{\text{Pa}(i)}$ , is Lipschitz-continuous with respect to 1-Wasserstein distance (Bartl and Eckstein, 2025; Piening and Chung, 2024; Altekrüger et al., 2023; Bénézet et al., 2024). We prove this result in Proposition B.1.

In generative modeling, the assumptions given in (25) can be interpreted as follows: Let  $(\mathcal{Z}, \mathcal{F}, \nu)$  be a probability space,  $\mathcal{X}_{\text{Pa}(i)} \subset \mathbb{R}^m$  and  $g : \mathcal{X}_{\text{Pa}(i)} \times \mathcal{Z} \rightarrow \mathbb{R}^d$ . We assume that for every  $\mathbf{x}_{\text{Pa}(i)} \in \mathcal{X}_{\text{Pa}(i)}$ , the map  $z \mapsto g(\mathbf{x}_{\text{Pa}(i)}, z)$  is measurable and  $g(\mathbf{x}_{\text{Pa}(i)}, \cdot)_{\#}\nu \in \mathcal{P}_1(\mathbb{R}^d)$ , and for any  $\mathbf{x}_{\text{Pa}(i)}, \mathbf{x}'_{\text{Pa}(i)} \in \mathcal{X}_{\text{Pa}(i)}$  and all  $z \in \mathcal{Z}$ ,  $\|g(\mathbf{x}_{\text{Pa}(i)}, z) - g(\mathbf{x}'_{\text{Pa}(i)}, z)\| \leq C d_{\mathcal{X}_{\text{Pa}(i)}}(\mathbf{x}_{\text{Pa}(i)}, \mathbf{x}'_{\text{Pa}(i)})$ . Then, a measurable generator with finite first moment and uniform Lipschitz dependence on the conditioning random vector induces a  $W_1$ -Lipschitz family of conditional distributions, see Arjovsky et al. (2017); Papamakarios et al. (2021). This is proved in Appendix B.

Therefore, the assumption given (25) expresses a quantitative stability property of the model: small perturbations of the conditioning variables induce proportionally small changes in the corresponding conditional distributions in 1-Wasserstein distance. This stability naturally arises when conditional distributions are represented as the pushforwards of a reference noise distribution through generators that are Lipschitz in their conditioning variables.

## 6 INFIMAL SUBADDITIVITY IN ACTION

Section 5 shows that when the target distribution factorizes according to a known Bayesian network over a graph  $G$ , the corresponding global objective function can be related to a sum of lower-dimensional objective functionals defined on graph-informed families. In adversarial learning terms, this suggests replacing a graph-agnostic GAN with a monolithic discriminator by a graph-informed GAN with localized discriminators acting on families of variables. The aim of this section is to show how the graph-informed strategy behaves in practice across a range of structured target distributions. In particular, we find that graph-informed GANs often improve optimization stability and the recovery of the underlying conditional structure, while also revealing trade-offs between family-level and global distributional discrepancy, and between predictive accuracy and computational cost.

We study four case studies. The first two are synthetic continuous examples. The structured linear-Gaussian model, introduced in Section 5, serves as a controlled testbed in the sense that the graph structure is known and the effect of localization can be examined directly. In what follows, we complement the earlier objective-level results with additional diagnostics for global versus local error and with an experiment on the role of the Lipschitz constant. The second synthetic example is a ball-throwing time-series model (Ding et al., 2021, see, e.g., §8.1), which we use to examine training dynamics and convergence in the structured continuous setting.

The remaining two case studies use real discrete Bayesian networks, namely, CHILD from Spiegelhalter (1992) and EARTHQUAKE from Pearl (1988). We use CHILD to study structural fidelity and the effect of family size in a medium-sized network, and EARTHQUAKE to assess robustness across many runs in a smaller network.

The remainder of this section is organized as follows. We first describe the common training framework shared across the experiments, including the localized discriminator construction, objective functions, and validation metrics. We then present the synthetic case studies, followed by the real-world Bayesian network experiments.

### 6.1 COMMON EXPERIMENTAL FRAMEWORK

All four case studies train a generator to match a target distribution  $Q$  through a variational min–max objective of the form,

$$\inf_{P_\theta} \mathfrak{D}_f^\Gamma(Q \| P_\theta) = \inf_{P_\theta} \sup_{\gamma_\eta \in \Gamma} \left\{ E_Q[\gamma_\eta(x)] - \inf_{\nu \in \mathbb{R}} \{ \nu + E_{P_\theta}[f^*(\gamma_\eta(x) - \nu)] \} \right\}, \quad (20)$$

where  $\theta$  and  $\eta$  denote the generator and discriminator parameters, respectively. In the graph-agnostic setting, a single monolithic discriminator acts on the full sample vector. In the graph-informed setting, the discriminator is replaced by a collection of localized discriminators acting on lower-dimensional families of variables.

**Localized discriminators.** Recall that  $V$  denotes the full set of vertices in the DAG and hence  $|V| = n$  denotes the number of variables and that  $\mathbf{x}$  denotes a full sample from either the target or generated distribution. Given a collection of families  $F_1, \dots, F_n$ , with  $F_i \subset V$  for all  $i \in V$ , we associate to each  $F_i$  a discriminator

$$\gamma_{\eta_i}^i = \gamma^i(\cdot; \eta_i) : \mathcal{X}_{F_i} \rightarrow \mathbb{R}, \quad i = 1, \dots, n,$$

which acts only on subvectors  $\mathbf{x}_{F_i}$ . In the graph-informed experiments, these families are chosen to align with the structure of the Bayesian network. In the simplest case, they are the child–parent families  $F_i = \{i\} \cup \text{Pa}(i)$ . For discrete Bayesian networks, we generate a dummy encoding of each variable; if  $e(v)$  is the block of encoded coordinates for variable  $v$ , then we define encoded families  $\bar{F}_i = \cup_{v \in F_i} e(v)$  induced by  $F_i$  and the discriminators act on these encoded families  $\gamma^i : \mathcal{X}_{\bar{F}_i} \rightarrow \mathbb{R}$ .

**Local objectives.** For each localized discriminator, we define an objective functional comparing the corresponding marginals of real and generated samples. We consider two forms. For continuous experiments based on the KL-divergence, we use the Donsker–Varadhan representation,

$$\mathcal{J}_{\text{DV}}^i(\theta, \eta_i) = E_Q[\gamma^i(\mathbf{x}_{F_i}; \eta_i)] - \log E_{P_\theta}[\exp(\gamma^i(\mathbf{x}_{F_i}; \eta_i))]. \quad (21)$$

For the discrete experiments, we use the  $f$ -GAN form Nowozin et al. (2016),

$$\mathcal{J}_f^i(\theta, \eta_i) = E_Q[\gamma^i(\mathbf{x}_{\bar{F}_i}; \eta_i)] - E_{P_\theta}[f^*(\gamma^i(\mathbf{x}_{\bar{F}_i}; \eta_i))], \quad (22)$$

where  $f^*$  is the convex conjugate corresponding to the chosen  $f$ -divergence (see Section 3.2). In the latter case, the output activation of each discriminator is chosen so that its values lie in the effective domain of  $f^*$ . Note that for the KL-divergence, (21) is a special case of (20) after optimizing over  $\nu$ , whereas the  $f$ -GAN formulation in (22) corresponds to fixing  $\nu$  and therefore changes the gradients and training dynamics.

**Global graph-informed objective.** Training is performed by summing the local objectives,

$$\mathcal{J}(\theta, \eta_1, \dots, \eta_n) = \sum_{i=1}^n w_i \mathcal{J}^i(\theta, \eta_i). \quad (23)$$

When all families correspond to the child–parent families, the choice  $w_i = 1/n$  matches the averaged form suggested by the infimal subadditivity results up to a constant normalization. Algorithm 1 summarizes the resulting training scheme.

**Continuous and discrete generators.** For continuous data, the generator outputs  $\tilde{\mathbf{x}} \sim P_\theta$  directly from the latent noise  $\mathbf{z} \sim P_Z$ . For discrete Bayesian networks, the generator outputs logits for each categorical variable block, and differentiable relaxed samples are obtained by applying Gumbel–softmax (Jang et al., 2017) to each block before evaluation by the discriminators.

**Restricting the discriminator class.** In the experiments that consider an interpolative divergence, we impose a Lipschitz-type restriction on each discriminator via spectral normalization to every dense layer (Miyato et al., 2018). This yields the class of constrained discriminators used in the numerical studies and is particularly important in the continuous KL-based experiments, where it prevents degenerate discriminator behavior.

**Validation metrics.** Across the experiments, we monitor the variational objective together with global, local, and case-specific validation diagnostics. Global distributional fit is assessed using energy distance (Székely and Rizzo, 2013). For the discrete Bayesian network experiments, where the target conditional probability tables (CPTs) are known, we additionally report the average log-likelihood of generated samples under the ground-truth Bayesian network. Local fit is assessed using the area under the receiver operating characteristic curve (AUC) for each discriminator, while further structure-specific diagnostics are introduced in the relevant case studies.

**Algorithm 1:** Graph-informed variational training with localized discriminators

**Input:** Target  $Q$ ; latent noise  $P_Z$ ; generator  $\text{Gen}(\cdot; \theta)$ ; batch size  $B$ ; families  $F_1, \dots, F_n$ ;  
 local discriminators  $\gamma^1(\cdot; \eta_1), \dots, \gamma^n(\cdot; \eta_n)$ ; learning rates  $\ell_\eta, \ell_\theta$ ; weights  $w_1, \dots, w_n$ .  
**Choice:** Objective form (A) DV-KL or (B)  $f$ -GAN.

```

1 for training steps  $t = 0, 1, 2, \dots$  do
2   Sample minibatches  $\{\mathbf{x}^{(k)}\}_{k=1}^B \sim Q$  and  $\{\mathbf{z}^{(k)}\}_{k=1}^B \sim P_Z$ 
3   Form generated minibatch  $\{\tilde{\mathbf{x}}^{(k)}\}_{k=1}^B$ :
4   if categorical data then
5     // Generator outputs logits for each categorical variable
6     // block; relaxed samples are formed via Gumbel-softmax
7      $\tilde{\mathbf{x}}^{(k)} \leftarrow \text{GumbelSoftmax}_\tau(\text{Gen}(\mathbf{z}^{(k)}; \theta^t))$  for  $k = 1, \dots, B$ 
8   else
9      $\tilde{\mathbf{x}}^{(k)} \leftarrow \text{Gen}(\mathbf{z}^{(k)}; \theta^t)$  for  $k = 1, \dots, B$ 
10  Calculate objectives and update parameters:
11  for  $i = 1, \dots, n$  do
12    if (A) DV-KL then
13       $\hat{\mathcal{J}}^i \leftarrow \frac{1}{B} \sum_{k=1}^B \gamma^i(\mathbf{x}_{F_i}^{(k)}; \eta_i^t) - \log\left(\frac{1}{B} \sum_{k=1}^B \exp(\gamma^i(\tilde{\mathbf{x}}_{F_i}^{(k)}; \eta_i^t))\right)$  // see (21)
14    else if (B)  $f$ -GAN then
15       $\hat{\mathcal{J}}^i \leftarrow \frac{1}{B} \sum_{k=1}^B \gamma^i(\mathbf{x}_{F_i}^{(k)}; \eta_i^t) - \frac{1}{B} \sum_{k=1}^B f^*(\gamma^i(\tilde{\mathbf{x}}_{F_i}^{(k)}; \eta_i^t))$  // see (22)
16      // activation is chosen so that discriminator outputs
17      // lie in the effective domain of  $f^*$ 
18   $\hat{\mathcal{J}} \leftarrow \sum_{i=1}^n w_i \hat{\mathcal{J}}^i$  // see (23)
19  // One discriminator step per minibatch
20   $\eta_i^{t+1} \leftarrow \eta_i^t + \ell_\eta \nabla_{\eta_i} \hat{\mathcal{J}}(\theta^t, \eta_1^t, \dots, \eta_n^t)$  for  $i = 1, \dots, n$ 
21  // One generator step per minibatch
22   $\theta^{t+1} \leftarrow \theta^t - \ell_\theta \nabla_\theta \hat{\mathcal{J}}(\theta^t, \eta_1^t, \dots, \eta_n^t)$ 
23  Record validation and runtime diagnostics

```

For integrable random vectors  $\mathbf{x}, \mathbf{y} \in \mathbb{R}^d$ , the energy distance is

$$\mathcal{E}(\mathbf{x}, \mathbf{y}) = 2E|\mathbf{x} - \mathbf{y}|_d - E|\mathbf{x} - \mathbf{x}'|_d - E|\mathbf{y} - \mathbf{y}'|_d,$$

where  $\mathbf{x}'$  and  $\mathbf{y}'$  are independent copies. The energy distance is a natural, rotation-invariant extension of the Cramér–von Mises–Smirnov distance in higher dimensions, which compares between-group and within-group variability. We estimate  $\mathcal{E}$  between held-out real data and generated samples; for the discrete Bayesian network experiments, this is computed on the corresponding dummy-encoded sample vectors.

For the discrete Bayesian network experiments, the average log-likelihood evaluates how well generated samples agree with the ground-truth Bayesian network. Concretely, we sample from the generator, decode the categorical outputs, and evaluate the resulting configurations under the known joint probability distribution defined by the CPTs. Higher values indicate better agreement with the target distribution. Since the target Bayesian network is known in these experiments, this should be interpreted as an oracle diagnostic rather than as a likelihood for the generator itself.

For each discriminator, we also compute the AUC on held-out real versus generated samples restricted to the corresponding family. AUC values near 0.5 indicate that the generator matches the data well in the discriminator’s domain, whereas larger values indicate remaining discrepancy.

Finally, each case study uses additional structural diagnostics tailored to the example: parent-coefficient recovery in the structured Gaussian experiment, inferred gravitational constant and initial velocity in the ball-throwing experiment, and node-wise total variation error between generated and target marginals in the discrete Bayesian network experiments.

## 6.2 SYNTHETIC DATA

We consider two synthetic case studies for continuous Bayesian networks and assess the success of the graph-informed GANs using domain-grounded diagnostics. The first synthetic experiment uses the structured linear-Gaussian Hasse network from Figure 1 to isolate the effect of discriminator localization. In addition to the objective-level behavior discussed alongside Theorem 5.4, we use this example to assess whether graph-informed training preserves global distributional quality using the energy distance and how the objective functional dynamics depend on the Lipschitz constant. The second synthetic example is the ball-throwing time series, whose explicit conditional structure makes it useful for studying practical training dynamics and stability in a continuous setting.

### 6.2.1 STRUCTURED LINEAR-GAUSSIAN HASSE NETWORK

We revisit the structured linear-Gaussian model in (18) and Figure 1 that was introduced as a direct experimental testbed for Theorem 5.4. In this example, the generator is from a fixed parametric family and the true conditional structure is known, thereby separating the effect of discriminator localization from generator expressivity. Since the earlier discussion in Section 5 already established the main objective-level comparison, the additional diagnostics below show that localized discriminators aligned with the true Bayesian-network families, which improve the recovery of conditional and marginal distributions, do so while maintaining comparable global fit. We also illustrate how the Lipschitz restriction affects the resulting variational dynamics. Unless otherwise stated, the summaries for this case study are based on 13 paired runs per model; the Lipschitz constant study in Figure 3b is based on only 3 runs per model.

For each random seed, we first instantiate the Hasse Gaussian Bayesian network of the subset lattice of a three-element set using the edge weights  $\phi_{ji}$  shown in Figure 1. We then generate 32,000 i.i.d. observations by ancestral simulation. These are split into training and validation sets in a 90:10 ratio. All discriminator constructions are trained on the same instantiated network and the same train-validation split for a given seed, so that differences can be attributed to the discriminator design rather than to differences in the data-generating instance.

To isolate the role of discriminator localization, we fix the parametric family of the generator across all methods. In every case, the generator is a full-covariance Gaussian model

$$P_\theta = \mathcal{N}(\mu_\theta, \Sigma_\theta), \quad \Sigma_\theta = L_\theta L_\theta^\top,$$

with trainable parameters  $\theta = (\mu_\theta, L_\theta)$ . Thus, the comparison is not between more and less expressive generators, but between different variational objectives induced by different discriminator constructions. This is consistent with Theorem 5.4, where the optimization in (10) is over all candidate probability distributions  $P \in \mathcal{P}(\mathcal{X})$  and the graph-informed effect enters through the localized objective rather than through an explicit structural restriction on the generator.

Each discriminator is implemented as a neural network with two hidden layers, each with 16 units and Leaky ReLU activations, trained with the DV-KL objective (21). We report results for variational objectives based on both classical and interpolative divergences (i.e., Lipschitz-restricted). In the latter case, spectral normalization is applied to enforce a controlled Lipschitz constant, so that the discriminator class approximates a Lipschitz-bounded class. Training uses Adam with learning rates  $(\ell_\eta, \ell_\theta) = (10^{-3}, 3 \times 10^{-3})$ , a batch size of 256, and a maximum of 60 epochs, with early stopping triggered when the validation energy distance falls below 0.05 for five consecutive epochs.

The experiment seeks to compare three discriminator constructions. The first is a graph-agnostic baseline with a single monolithic discriminator acting on the full joint distribution. The second is a graph-informed model with one localized discriminator for each child-parent family  $F_i = \{i\} \cup \text{Pa}(i)$ . The third is a misaligned multi-discriminator baseline in which each true family is replaced by a size-matched subset that excludes the true parents. This misaligned construction is included to test whether any observed gains come from graph alignment itself rather than simply from distributing capacity across several smaller discriminators. For the graph-informed objectives, we use uniform weights across families, so that the overall objective is the average of the local DV terms.

In Section 5, we assessed the structural fidelity through recovery of the parent coefficients  $\{\phi_{ji}\}$  by regressing generated samples onto the true parent set and averaging the resulting  $L_2$  error over non-root nodes. Here we complement that local diagnostic with a global one, namely the energy distance

on the full eight-dimensional validation sample in Figure 3a. Taken together with Figure 2b, the full picture is that the graph-informed GAN improves parent-coefficient recovery while remaining competitive with the monolithic baseline in global energy distance. The misaligned multi-discriminator achieves energy-distance values of a similar order, but fails to recover the correct conditional structure. This shows that the benefit is not simply the use of several discriminators, but the use of discriminators aligned with the correct families.

Figure 3b illustrates how the evolution of the variational loss on the validation set changes as the Lipschitz constant  $L$  is varied for the graph-informed multi-discriminator construction, with the monolithic discriminator at  $L = 1$  included for reference. The plot shows the mean loss over the validation data, with a min-max envelope based on 3 runs for each model. Since the objective functional itself depends on  $L$ , this figure is best interpreted as showing differences in training dynamics and surrogate behavior rather than providing a direct comparison of absolute objective values across Lipschitz constants. This study shows that the local surrogate (17) changes meaningfully with the Lipschitz constant  $L$ . In particular, a smaller  $L$  produces a lower-valued and more rapidly decaying surrogate, while a larger  $L$  yields a higher-valued objective and slower decay.

In summary, this case study supports the interpretation of Theorem 5.4 in a controlled setting. The graph-informed GAN performs best on recovering the correct conditional mechanisms, while still maintaining competitive global distributional quality as compared to the graph-agnostic GAN. Moreover, the Lipschitz constant study shows that varying  $L$  alters both the objective’s magnitude and its training dynamics, suggesting that  $L$  can serve as a practical tuning parameter to balance regularization, stability, and sensitivity in graph-informed adversarial training.

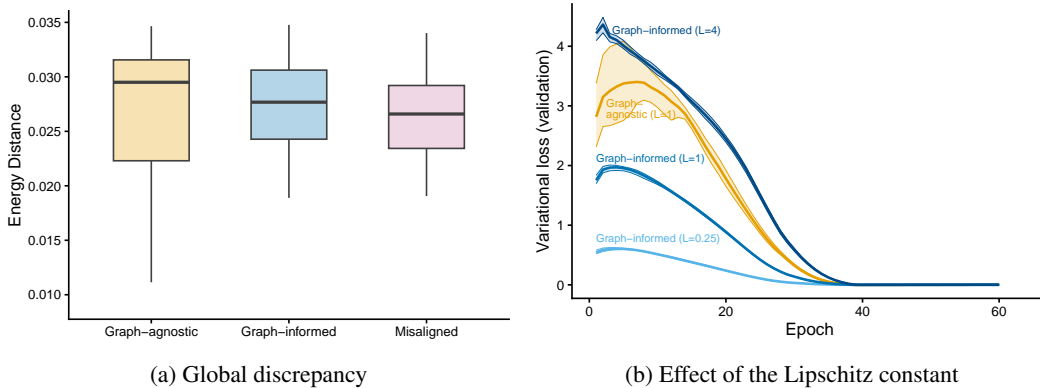


Figure 3: Additional diagnostics for the structured linear-Gaussian Hasse network, complementing the objective-level comparison in Figure 2. (a) Energy distance (lower is better) provides a global measure of distributional discrepancy across the three discriminator constructs under the Lipschitz-restricted interpolative divergence (cf. parent-coefficient recovery in Figure 2b); boxplots summarize 13 paired runs per model. (b) Variational loss for the graph-informed GAN trained using an interpolative divergence at several Lipschitz constants  $L$ , with the graph-agnostic GAN at  $L = 1$  for reference; mean with a min-max envelope based on 3 runs per model.

### 6.2.2 BALL-THROWING TRAJECTORY

We use the synthetic ball-throwing trajectory to study graph-informed adversarial training in a continuous setting where the main issue is practical trainability rather than objective-level certification as in the previous experiment. In this example, the underlying dependence structure is explicit, and the generated trajectories admit physically interpretable diagnostics through the gravitational constant and initial velocity recovered from fitted trajectories. The experiment therefore serves two purposes: it shows how the Lipschitz restriction naturally stabilizes the training, and it tests whether replacing a graph-agnostic monolithic discriminator by graph-informed localized discriminators yields smoother and more diagnostically useful training dynamics. Unless otherwise stated, the summaries in Figure 5 are based on 20 independent runs per model for the interpolative setting and 10 independent runs per model for the classical setting.

The target probability distribution  $Q$  is the joint distribution of a discretized collection of ball trajectories with random initial velocities. For a ball with unit mass, the gravitational acceleration  $g$ , and an initial velocity  $v_0$ , the trajectory is

$$y_t = v_0 t - \frac{1}{2} g t^2. \quad (24)$$

For each independent  $v_0 \sim N(\mu_v, \sigma_v^2)$ , we observe the time series

$$\mathbf{y} = (y_{t_0}, y_{t_1}, \dots, y_{t_m}), \quad t_j = j/m, \quad j = 0, \dots, m,$$

at  $m + 1 = 15$  uniformly spaced time points in  $[0, 1]$ . In the experiments below, we use  $\mu_v = 4$  and  $\sigma_v = 3$ . Figure 4 shows fifty representative trajectories from the target distribution together with generated trajectories from graph-informed and graph-agnostic models.

As (24) is a second-order equation in time, the resulting joint probability distribution has a natural local dependence structure: conditional on the two previous positions, the next position is determined up to the randomness induced by  $v_0$ . This motivates the Bayesian network description,

$$y_{t_{j-1}} \rightarrow y_{t_j} \leftarrow y_{t_{j-2}}, \quad j = 2, \dots, m,$$

together with the boundary relation  $y_{t_0} \rightarrow y_{t_1}$ . In the graph-informed model, the localized discriminator families are chosen to reflect this structure. In particular, the families correspond to triples of the form  $(y_{t_j}, y_{t_{j-1}}, y_{t_{j-2}})$ , with the obvious truncation near the initial time.

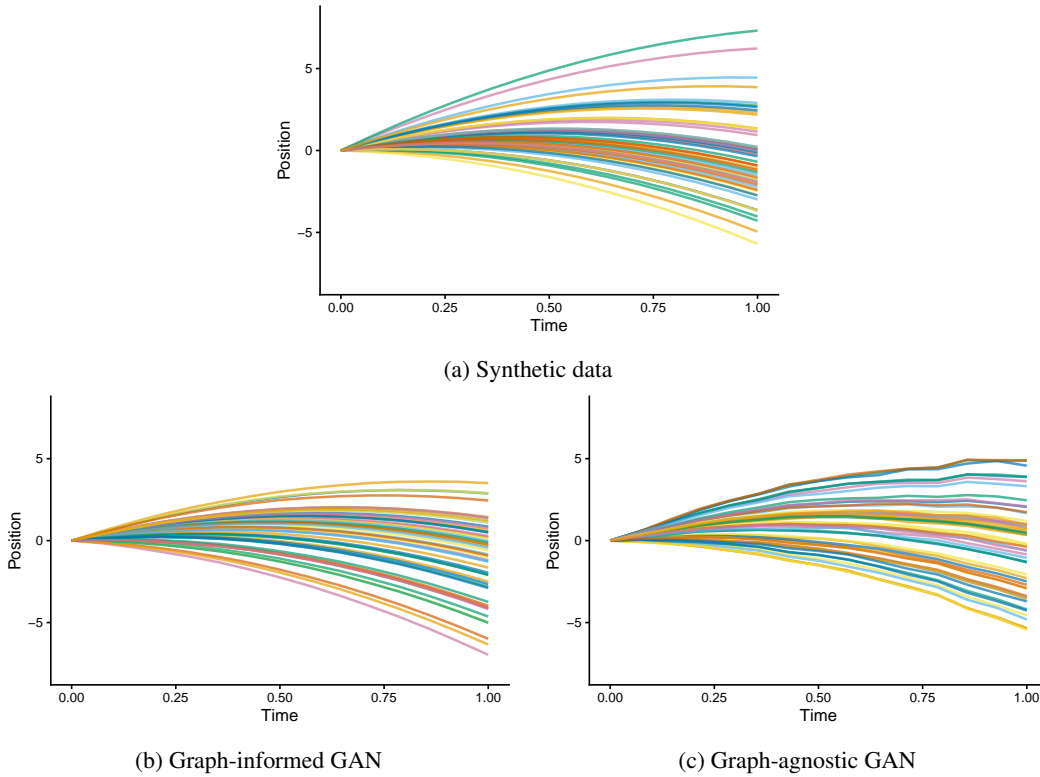


Figure 4: Fifty ball-throwing trajectory time series from various distributions. (a) Samples from the target distribution with  $v_0 \sim N(\mu_v = 4, \sigma_v^2 = 3^2)$ . (b) Fifty generated trajectories from a graph-informed GAN with 14 localized discriminators trained using an interpolative divergence with a Lipschitz constraint. (c) Fifty generated trajectories from a graph-agnostic GAN with a monolithic discriminator trained using an interpolative divergence with a Lipschitz constraint.

We compare a graph-agnostic model, with a single monolithic discriminator acting on the full trajectory, against a graph-informed model, with 14 localized discriminators aligned with the Bayesian-network child-parent families. The discriminators are fully connected networks with two hidden

layers of width 32 and Leaky ReLU activations. Both models use the same generator architecture (a fully-connected feed-forward network with latent dimension 64, two hidden layers of width 128, and swish activations, outputting a length-15 trajectory) and are trained with the Donsker–Varadhan form of the KL objective in (21) with minibatches of size 256 using Adam with one discriminator update and one generator update per minibatch with learning rates  $(\ell_\eta, \ell_\theta) = (5 \times 10^{-4}, 10^{-3})$ . To assess the role of interpolative regularization, we also compare training with and without spectral normalization. In the constrained setting, spectral normalization is applied to each discriminator layer so that the discriminator class approximates a Lipschitz-bounded class; in the unconstrained setting, the same discriminator architecture is trained directly without this restriction.

The generated trajectories also admit interpretable physics-based diagnostics. By fitting the quadratic model in (24) to generated samples via least squares, we obtain estimates  $\hat{v}_0$  and  $\hat{g}$  from the fitted linear and quadratic coefficients. We track the empirical mean and spread of these estimates across generated samples, as a good model should reproduce both the distribution of initial velocities and the true gravitational constant, not merely match the trajectories in a generic distributional sense. These physics-based diagnostics provide an interpretable validation signal for model selection and early stopping.

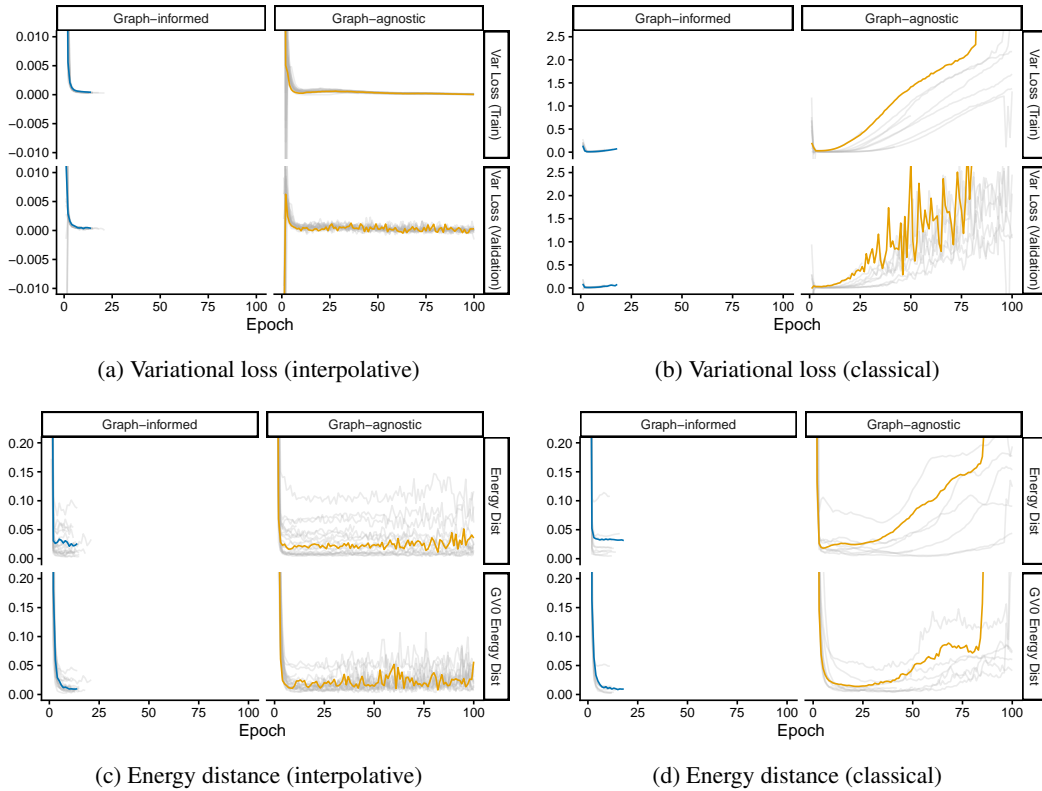


Figure 5: Training diagnostics for the ball-trajectory experiment from a representative run; the graph-informed GAN with 14 localized discriminators aligned to child–parent families in the Bayesian network is compared to the graph-agnostic GAN with a monolithic discriminator. (a) and (b) show the evolution of the KL variational loss (21) on the training and validation sets, for an interpolative (20 runs in total) and classical divergence (10 runs in total), i.e., with and without Lipschitz constraints enforced via spectral normalization. (c) and (d) show the corresponding energy-distance diagnostics, both for the full trajectory distribution and for the recovered physics parameters  $(\hat{g}, \hat{v}_0)$ , again for an interpolative and classical divergence.

Figure 5 summarizes the main training diagnostics. Panels (a) and (b) show the evolution of the variational objective with and without the Lipschitz restriction. When using an interpolative divergence, both graph-informed and graph-agnostic training remain numerically stable and produce interpretable loss curves. Without this restriction, the DV–KL objective becomes much less well

behaved, reflecting the instability of the log-moment term in the unconstrained setting. Panels (c) and (d) show the corresponding energy-distance diagnostics. The main qualitative effect is that the interpolative restriction stabilizes training, while graph-informed localization makes the validation curves less oscillatory and therefore easier to use for model monitoring and stopping.

This stabilization is especially visible when comparing the graph-informed model with the graph-agnostic model. Although the localized model updates multiple discriminators per minibatch, its training curves are smoother, and the inferred physics is more stable across epochs. In this example, the benefit of graph-informed localization is a more reliable optimization process and a clearer diagnostic picture under a comparable wall-clock budget.

Overall, the ball-throwing experiment complements the Hasse-network study by highlighting a different advantage of graph-informed training. In the Hasse example, the main gain was improved structural recovery under a known Bayesian-network factorization. Here, the main illustrated gain is improved practical trainability in a structured continuous model: the interpolative restriction prevents DV-KL degeneracy, and graph-informed localized discriminators yield smoother and more interpretable training dynamics than a graph-agnostic monolithic discriminator.

### 6.3 REAL-WORLD BAYESIAN NETWORKS

We now turn to two real-world Bayesian networks in order to study graph-informed adversarial training beyond the synthetic continuous setting. The first example uses the CHILD network from Spiegelhalter (1992), a medium-sized Bayesian network consisting of 20 categorical variables and 25 directed edges (230 parameters) that describe clinical factors associated with birth asphyxia (Figure 6a). The second example uses the EARTHQUAKE network from Pearl (1988) (see also Korb and Nicholson (2010)), a smaller Bayesian network consisting of 5 nodes and 4 directed edges (10 parameters). In both cases, the network structure and CPTs are assumed to be known. These experiments are intended to test whether the graph-informed GAN continues to improve structural fidelity in discrete settings, and whether the resulting multi-discriminator training remains stable across repeated runs.

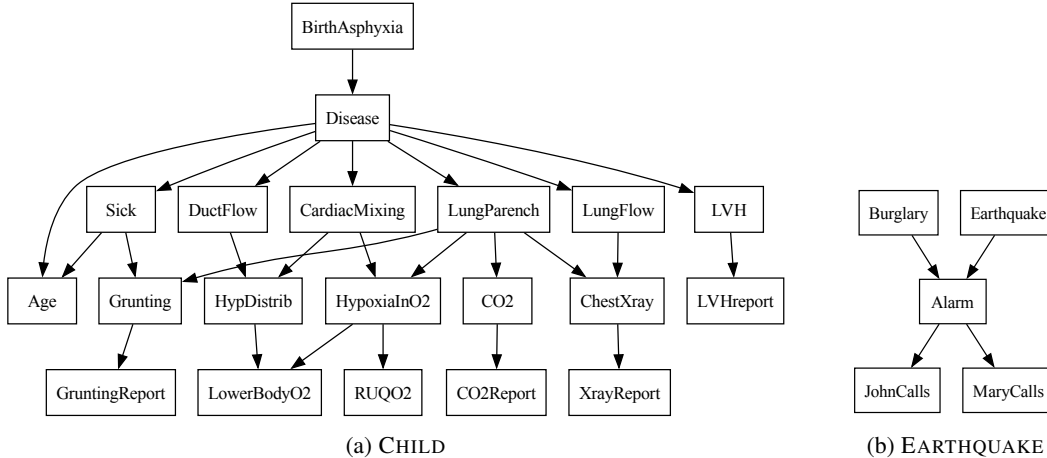


Figure 6: The two real-world discrete Bayesian networks used in the experiments. (a) CHILD, a medium-sized, discrete Bayesian network with 20 nodes and 25 arcs (230 parameters) describing a possible diagnostic tool for birth asphyxia for newborn babies with congenital heart disease, from Spiegelhalter (1992). (b) EARTHQUAKE, a small-sized, discrete Bayesian network consisting of 5 nodes and 4 arcs (10 parameters), from Pearl (1988); Korb and Nicholson (2010).

#### 6.3.1 LOCALIZATION FOR DISCRETE BAYESIAN NETWORKS

Since CHILD and EARTHQUAKE are fully discrete, we employ a differentiable relaxation to enable gradient-based training. The generator outputs a single dummy-encoded vector of logits, partitioned into blocks corresponding to the categorical variables. We obtain differentiable samples by applying the Gumbel–softmax relaxation of Jang et al. (2017) independently to each block. Gumbel noise is

added to the logits, and a temperature-controlled softmax produces an approximate dummy encoding per variable. These relaxed samples are passed to the discriminators during training, while hard-decoded samples are used for diagnostics.

All models in this section are trained with an interpolative JS-Wasserstein-type objective. That is, we consider the graph-informed objective in (23), using the  $f$ -GAN form in (22) with the JS divergence and layer-wise spectral normalization in the discriminator to enforce a Lipschitz constraint.

The diagnostics reflect that the target Bayesian networks are fully known. We monitor the variational objective during training, the energy distance on held-out validation samples, and the average log-likelihood of generated samples under the known conditional probability tables. Since this log-likelihood is evaluated under the ground-truth Bayesian network rather than under the generator itself, it should be interpreted as a measure of agreement with the target probability distribution. To assess local fit, we report discriminator AUC values on held-out real versus generated samples. We also compute node-wise total variation error between generated marginals and the corresponding target marginals.

### 6.3.2 CHILD

The CHILD experiment assesses the graph-informed GAN on a medium-sized discrete Bayesian network in the theory-aligned child–parent setting and examines how the size of the localized discriminator families affects the trade-off between local and global fit of model predictions. We report results over 15 independent runs.

For each CHILD run, we draw 64,000 i.i.d. cases from the exact Bayesian network by ancestral sampling, dummy-encode the resulting categorical observations into a 60-dimensional vector, and split the data 90:10 into training and validation sets. The generator is a fully connected network with latent dimension 32, hidden widths (64, 64, 64, 64), swish activations, and a linear output layer producing logits for all dummy variables. The discriminators are fully connected networks with hidden widths (16, 8, 4) and Leaky ReLU activations. Training uses Adam with learning rates  $(\ell_\eta, \ell_\theta) = (5 \times 10^{-4}, 5 \times 10^{-5})$ , batch size 512, and at most 150 epochs, with early stopping based on the validation average log-likelihood under the ground-truth CPTs (patience 20, minimum improvement  $10^{-3}$ ), after which the best checkpoint is restored. The graph-agnostic baseline uses a single discriminator on the full 60-dimensional dummy vector. The graph-informed model uses 20 localized discriminators aligned with the network families.

For CHILD, we write  $M$  for the graph-agnostic GAN model with a monolithic discriminator, and  $M_a$  for the graph-informed GAN model with localized discriminators acting on the families of ancestor depth  $a$ ,

$$F_i^{(a)} = \{i\} \cup \text{An}_{\leq a}(i),$$

where  $\text{An}_{\leq a}(i)$  denotes the ancestors of  $i$  within graph distance at most  $a$ . In particular,  $a = 1$  corresponds to the typical child–parent family  $F_i^{(1)} = \{i\} \cup \text{Pa}(i)$ . We compare the graph-agnostic model  $M$  with the graph-informed models  $M_1$  and  $M_3$ .

The model  $M_1$  aligns with the graph-informed child–parent families covered by our main framework. By contrast, the model  $M_3$  is included as an exploratory extension motivated by Remark 5.12. This larger family localization is not presented as a direct consequence of Theorem 5.4, but rather as a way to examine how broader family-aligned neighborhoods affect the discriminator’s inductive bias.

Figure 7a first shows that graph-informed training produces smoother variational-loss curves than the graph-agnostic baseline. Empirically,  $M_3$  tends to occupy an intermediate regime between the more local graph-informed model  $M_1$  and the monolithic graph-agnostic model  $M$ . Both  $M_1$  and  $M_3$  exhibit less oscillatory training and validation behavior than  $M$ , which makes convergence easier to diagnose. This mirrors the stabilization effects already observed in the continuous experiments, but now in a discrete setting using the interpolative JS objective functional.

The global validation metrics in Figure 8a show that localization changes the balance between local and global fit. The graph-informed models typically achieve higher average log-likelihood under the ground-truth Bayesian network than the graph-agnostic baseline, indicating better agreement with the known conditional structure. The energy distance, however, does not improve uniformly:

model  $M_1$  can yield slightly worse global energy distance than the monolithic baseline, while the model  $M_3$  typically lies between the two. This is consistent with the view that larger neighborhoods recover more of the global dependence structure, whereas smaller families place greater emphasis on local fidelity.

This local advantage is reflected more clearly in the discriminator AUC and total-variation diagnostics. In Figure 8c, the AUC values for the localized discriminators in  $M_1$  and  $M_3$  move more consistently toward 0.5 on their respective families than does the monolithic discriminator in  $M$  on the full joint space. For reference, the displayed critics correspond to the nodes BirthAsphyxia ( $D_0$ ), HypoxiaInO2 ( $D_2$ ), XrayReport ( $D_{10}$ ), CardiacMixing ( $D_{16}$ ), and Sick ( $D_{19}$ ); see Figure 6a. The node-wise total-variation errors in Figure 9b show the same pattern. Although all fitted models achieve relatively small marginal errors, the graph-informed models reduce these errors systematically, with  $M_1$  attaining the lowest mean node-wise total variation across runs in Figure 9a.

The CHILD experiment shows that on a medium-sized discrete Bayesian network, graph-informed localization improves structural fidelity, as directly reflected in node-wise total variation, local AUC, and log-likelihood. Broader neighborhoods partly recover global fit, but the main advantage of the graph-informed GAN in this setting is better alignment with the conditional structure encoded by the Bayesian network.

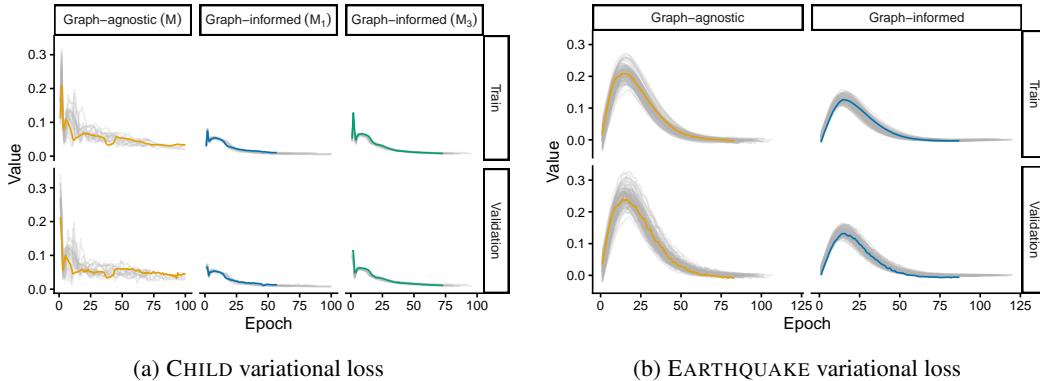


Figure 7: Training and validation variational loss (interpolative JS-Wasserstein) for the real-world discrete Bayesian network experiments. (a) Compares the graph-agnostic GAN model  $M$  with the graph-informed GAN models  $M_1$  (child–parent families) and  $M_3$  (ancestor depth-3 families) on CHILD over 15 runs. (b) Compares the graph-agnostic GAN and the graph-informed GAN on EARTHQUAKE over 85 runs.

### 6.3.3 EARTHQUAKE

The EARTHQUAKE experiment serves a different purpose from CHILD. Because the network is small, the graph-agnostic GAN with a monolithic discriminator is already operating in a relatively low-dimensional setting, so the main question is not whether localization dramatically improves the average metric values, but whether it improves reliability across repeated runs. Here we compare the graph-agnostic model with the graph-informed model using the child–parent families and report results over 85 independent runs.

For each EARTHQUAKE run, we draw 8,000 i.i.d. cases from the exact Bayesian network by ancestral sampling, dummy-encode them into a 10-dimensional vector, and use a 90:10 train–validation split. The generator is a fully connected network with latent dimension 16, two hidden layers with widths 32, swish activations, and linear output logits. The discriminators are fully connected networks with two hidden layers also with widths 32 and Leaky ReLU activations. Training uses Adam with learning rates  $(\ell_\eta, \ell_\theta) = (10^{-4}, 5 \times 10^{-5})$ , batch size 256, and at most 120 epochs, with early stopping based on the validation average log-likelihood under the ground-truth CPTs, after which the best checkpoint is restored. The graph-agnostic baseline uses one discriminator on the full 10-dimensional dummy vector, whereas the graph-informed model uses 5 localized discriminators aligned with the child–parent families; the corresponding family input widths range from 2 to 6 dummy coordinates.

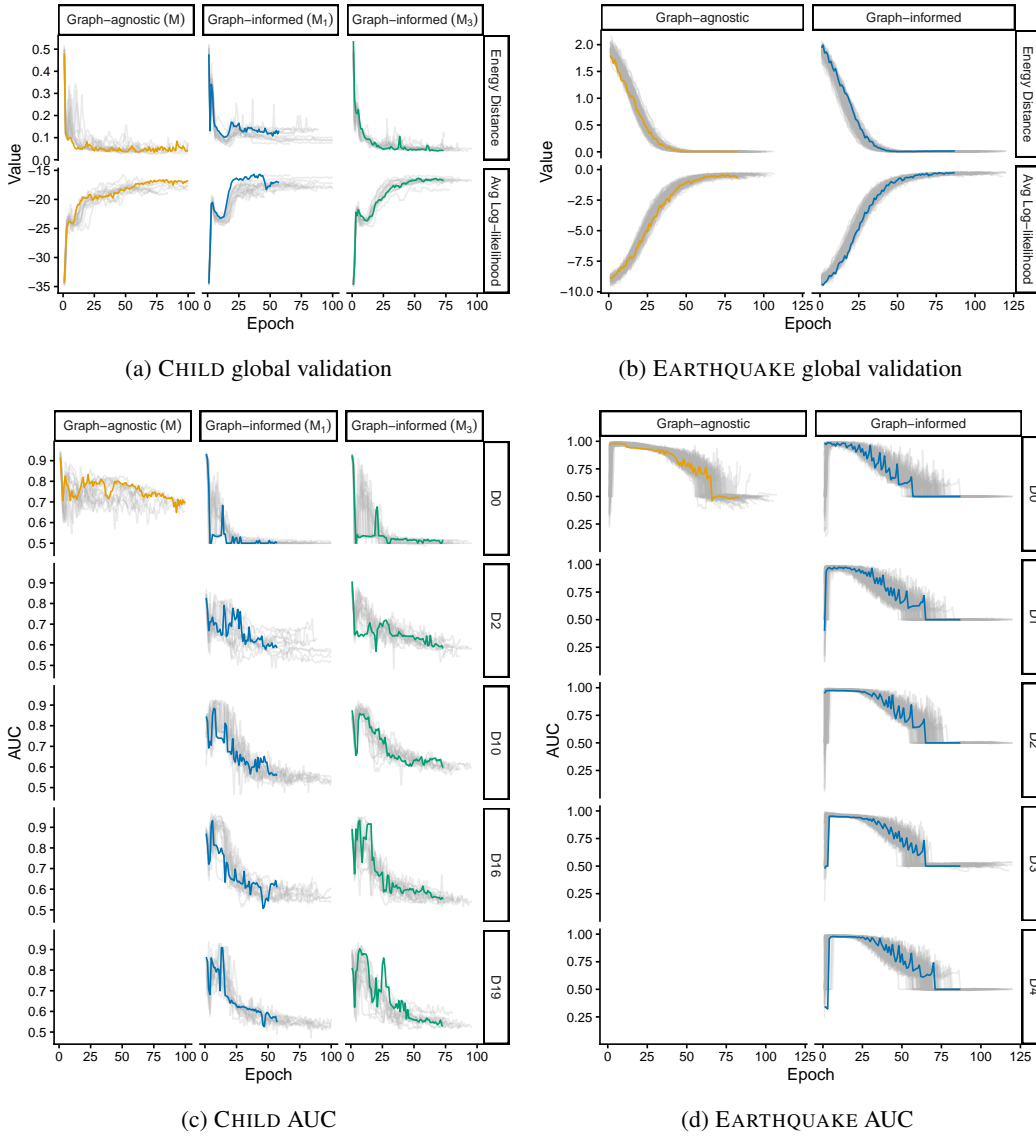


Figure 8: Validation diagnostics for the real-world discrete Bayesian network experiments (single run highlighted). The CHILD experiment compares  $M$ ,  $M_1$ , and  $M_3$ , corresponding to graph-agnostic GAN and two graph-informed GANs with child-parent and ancestor depth-3 families over 85 runs. The EARTHQUAKE experiment compares graph-agnostic and graph-informed GANs over 85 runs. (a) and (b) show global validation metrics, namely energy distance and average log-likelihood. (c) and (d) show representative discriminator AUC values.

Figure 7b again shows smoother training dynamics for the graph-informed GAN than for the graph-agnostic GAN. The difference is less dramatic than for CHILD, but the graph-informed model still exhibits less erratic variation in the training and validation objectives. In the global validation metrics shown in Figure 8b, the two models are broadly comparable in terms of their central tendency. This is consistent with the fact that the full joint distribution is small enough that the monolithic discriminator is not severely disadvantaged.

The main difference between the graph-agnostic and graph-informed models appears in robustness. In Figure 8d, the graph-informed discriminator AUC behaves more consistently across runs, while the monolithic baseline exhibits more variable behavior. The same effect is visible in the node-wise total-variation errors in Figure 9c: although the average performance of the two approaches is sim-

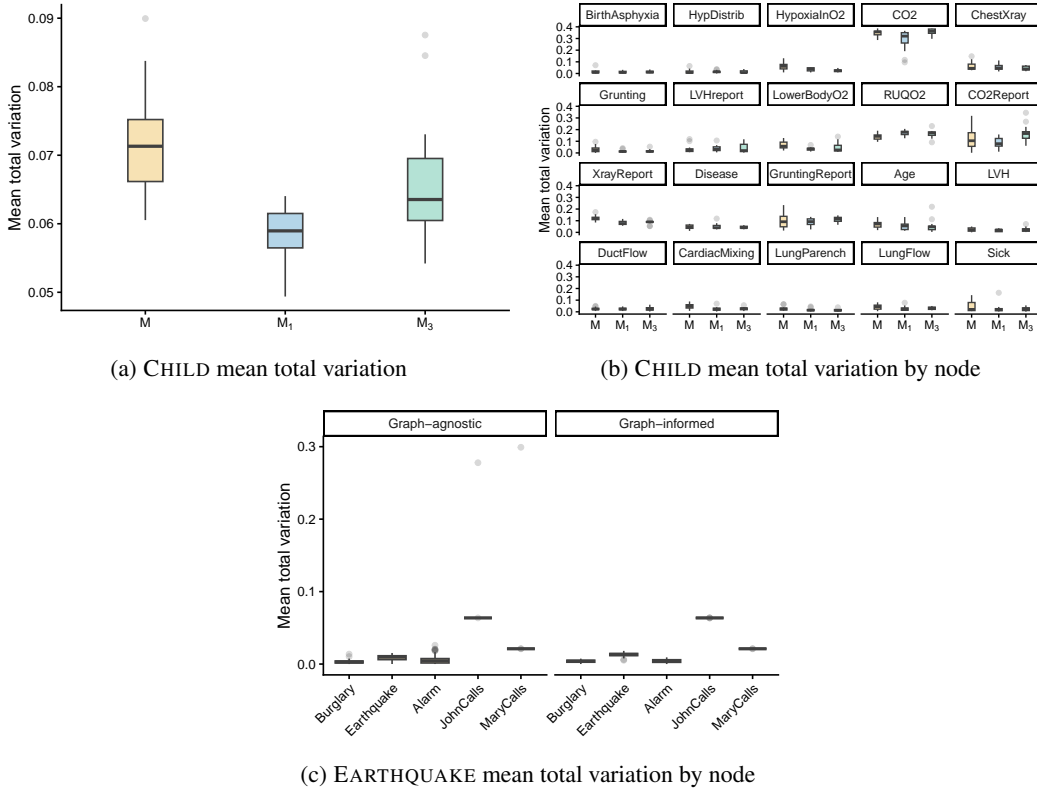


Figure 9: Total variation error between generated marginals and the corresponding target marginals from the known CPT. (a) The mean error by node by depth, across 15 runs for CHILD for graph-agnostic model  $M$  and graph-informed models  $M_1$  and  $M_3$ . (b) The mean error, averaged over all nodes by depth, across 15 runs for CHILD, highlighting variables such as CO2 with high error relative to other nodes. (c) The mean error by depth by node, across 85 runs for EARTHQUAKE; note the outliers in the graph-agnostic predictions.

ilar, the graph-agnostic model exhibits several more pronounced outliers. Thus, for EARTHQUAKE, the principal gain from graph-informed localization is not uniformly better average accuracy but improved reliability and fewer pathological runs.

This provides a useful boundary case for the broader conclusions of the paper. When the joint space is small, the graph-informed GAN still offers a practical advantage by making training more stable and reducing the frequency of poor outcomes across repeated runs.

## 7 DISCUSSION

We have introduced an infimal subadditivity principle for interpolative divergences on Bayesian networks and used it to give a variational justification for graph-informed adversarial learning. In particular, Theorems 5.4, 5.6, and 5.7 show that, when the target distribution factorizes according to a known DAG, a global discrepancy objective functional can be controlled by an average of family-level objective functionals aligned with the graph. This provides a principled basis for replacing a graph-agnostic GAN with a monolithic discriminator by a *graph-informed GAN* with localized discriminators, without requiring the optimizer itself to factorize according to the same graph. The same variational framework applies to  $(f, \Gamma)$ -divergences,  $\Gamma$ -IPMs, and proximal optimal transport divergences, and applies to natural discriminator classes including bounded measurable and Lipschitz-bounded functions.

The experiments suggest that the practical value of graph-informed adversarial learning is not only computational. Across the synthetic and real-world case studies, localization often improves train-

ing stability, reduces variability across runs, and yields better recovery of the underlying conditional structure in the generated distribution. At the same time, the CHILD experiments with “extended families” suggest that the choice of family size, or more generally of the graph-informed neighborhoods, mediates a trade-off between local structural fidelity and global distributional fit. This complements Remark 5.12: broader neighborhoods may tighten the surrogate and recover more of the global dependence structure, but they may also reduce some of the advantages of strict localization in terms of simplicity, efficiency, and interpretability. “Learning big” with a single monolithic discriminator versus “learning small” with localized family-level discriminators should be viewed as a task-dependent modeling choice.

A related point is that localization also improves diagnosability. Because the graph-informed objective decomposes into family-level terms, the resulting training procedure naturally produces local, family-specific diagnostics, such as discriminator AUCs and node-wise errors. As seen in the experiments, these quantities can make it easier to identify where the model is failing to train, rather than only indicating that the full-joint fit remains inadequate. This is potentially valuable in structured applications where understanding which part of the distribution is poorly learned may matter as much as aggregate performance. From this perspective, graph-informed adversarial learning offers not only a computational decomposition of a difficult high-dimensional testing problem, but also a more interpretable diagnostic interface for model development which may be especially relevant in structured and potentially high-consequence applications.

Finally, our theory distinguishes between structured objectives and structured generators. The surrogate controls a global objective functional without requiring the optimizer itself to be explicitly restricted to  $\mathcal{P}^G$ , and this separation is one of the main conceptual advantages of the infimal formulation. It would therefore be natural to study how graph-informed discriminator design interacts with generators that are themselves structurally constrained, and whether combining both sides can yield sharper guarantees, improved sample efficiency, or better-calibrated uncertainty. More broadly, it would be interesting to better understand how the choice of neighborhoods, discrepancy class, and discriminator regularity should be adapted to the scientific or decision-making task at hand. In this sense, the present work should be viewed less as prescribing a single graph-informed architecture and more as establishing a general variational framework for learning with known probabilistic structure.

## REFERENCES

- Kartik Ahuja, Prasanna Sattigeri, Karthikeyan Shanmugam, Dennis Wei, Karthikeyan Natesan Ramamurthy, and Murat Kocaoglu. Conditionally independent data generation. In *Uncertainty in Artificial Intelligence*, pages 2050–2060. PMLR, 2021.
- Fabian Altekrüger, Paul Hagemann, and Gabriele Steidl. Conditional generative models are provably robust: Pointwise guarantees for bayesian inverse problems. *arXiv preprint arXiv:2303.15845*, 2023.
- Martin Arjovsky, Soumith Chintala, and Léon Bottou. Wasserstein generative adversarial networks. In *International conference on machine learning*, pages 214–223. PMLR, 2017.
- Yogesh Balaji, Rama Chellappa, and Soheil Feizi. Normalized wasserstein for mixture distributions with applications in adversarial learning and domain adaptation. In *Proceedings of the IEEE/CVF international conference on computer vision*, pages 6500–6508, 2019.
- Ricardo Baptista, Panagiota Birmpa, Markos A Katsoulakis, Luc Rey-Bellet, and Benjamin J Zhang. Proximal optimal transport divergences. *arXiv preprint arXiv:2505.12097*, 2025.
- Daniel Bartl and Stephan Eckstein. Fast wasserstein rates for estimating probability distributions of probabilistic graphical models. *arXiv preprint arXiv:2510.09270*, 2025.
- Cyril Bénézet, Ziteng Cheng, and Sebastian Jaimungal. Learning conditional distributions on continuous spaces. *arXiv preprint arXiv:2406.09375*, 2024.
- Jeremiah Birrell and Reza Ebrahimi. Optimal transport regularized divergences: Application to adversarial robustness. *arXiv preprint arXiv:2309.03791*, 2023.

- Jeremiah Birrell, Paul Dupuis, Markos A Katsoulakis, Yannis Pantazis, and Luc Rey-Bellet.  $(f, \gamma)$ -divergences: Interpolating between  $f$ -divergences and integral probability metrics. *Journal of machine learning research*, 23(39):1–70, 2022a.
- Jeremiah Birrell, Markos A Katsoulakis, Luc Rey-Bellet, and Wei Zhu. Structure-preserving gans. *arXiv preprint arXiv:2202.01129*, 2022b.
- Jeremiah Birrell, Yannis Pantazis, Paul Dupuis, Markos A Katsoulakis, and Luc Rey-Bellet. Function-space regularized  $r$ - $\gamma$  divergences. *arXiv preprint arXiv:2210.04974*, 2022c.
- Michel Broniatowski and Amor Keziou. Minimization of  $\varphi$ -divergences on sets of signed measures. *Studia Scientiarum Mathematicarum Hungarica*, 43(4):403–442, 2006.
- Jorge Casajús-Setién, Concha Bielza, and Pedro Larranaga. Evolutive adversarially-trained bayesian network autoencoder for interpretable anomaly detection. In *International Conference on Probabilistic Graphical Models*, pages 397–408. PMLR, 2022.
- Ya-Liang Chang, Zhe Yu Liu, Kuan-Ying Lee, and Winston Hsu. Free-form video inpainting with 3d gated convolution and temporal patchgan. In *Proceedings of the IEEE/CVF international conference on computer vision*, pages 9066–9075, 2019.
- Ziyu Chen, Hyemin Gu, Markos A Katsoulakis, Luc Rey-Bellet, and Wei Zhu. Robust generative learning with lipschitz-regularized  $\alpha$ -divergences allows minimal assumptions on target distributions. *arXiv preprint arXiv:2405.13962*, 2024.
- Constantinos Daskalakis and Qinxuan Pan. Square hellinger subadditivity for bayesian networks and its applications to identity testing. In *Conference on Learning Theory*, pages 697–703. PMLR, 2017.
- Mucong Ding, Constantinos Daskalakis, and Soheil Feizi. Gans with conditional independence graphs: On subadditivity of probability divergences. In *International Conference on Artificial Intelligence and Statistics*, pages 3709–3717. PMLR, 2021.
- Hongwei Du, Jiamin Wang, Jian Hui, Lanting Zhang, and Hong Wang. Denseggn: universal and scalable deeper graph neural networks for high-performance property prediction in crystals and molecules. *npj Computational Materials*, 10(1):292, 2024.
- Paul Dupuis and Yixiang Mao. Formulation and properties of a divergence used to compare probability measures without absolute continuity. *ESAIM: Control, Optimisation and Calculus of Variations*, 28:10, 2022.
- Farzan Farnia, William W Wang, Subhro Das, and Ali Jadbabaie. Gat-gmm: Generative adversarial training for gaussian mixture models. *SIAM Journal on Mathematics of Data Science*, 5(1):122–146, 2023.
- Soheil Feizi, Farzan Farnia, Tony Ginart, and David Tse. Understanding gans: the lqg setting. *arXiv preprint arXiv:1710.10793*, 2017.
- Ruili Feng, Jie Xiao, Kecheng Zheng, Deli Zhao, Jingren Zhou, Qibin Sun, and Zheng-Jun Zha. Principled knowledge extrapolation with gans. In *International Conference on Machine Learning*, pages 6447–6464. PMLR, 2022.
- Ian J Goodfellow, Jean Pouget-Abadie, Mehdi Mirza, Bing Xu, David Warde-Farley, Sherjil Ozair, Aaron Courville, and Yoshua Bengio. Generative adversarial nets. *Advances in neural information processing systems*, 27, 2014.
- Hyemin Gu, Panagiota Birmpa, Yannis Pantazis, Luc Rey-Bellet, and Markos A Katsoulakis. Lipschitz-regularized gradient flows and generative particle algorithms for high-dimensional scarce data. *SIAM Journal on Mathematics of Data Science*, 6(4):1205–1235, 2024.
- Ishaan Gulrajani, Faruk Ahmed, Martin Arjovsky, Vincent Dumoulin, and Aaron C Courville. Improved training of wasserstein gans. *Advances in neural information processing systems*, 30, 2017.

- Stephanie Hyland, Cristóbal Esteban, and Gunnar Rätsch. Real-valued (medical) time series generation with recurrent conditional gans. *arXiv preprint arXiv:1706.02633*, 2018.
- Eric Jang, Shixiang Gu, and Ben Poole. Categorical reparametrization with gumbel-softmax. In *Proceedings International Conference on Learning Representations (ICLR)*, April 2017.
- Murat Kocaoglu, Christopher Snyder, Alexandros G Dimakis, and Sriram Vishwanath. Causalgan: Learning causal implicit generative models with adversarial training. *arXiv preprint arXiv:1709.02023*, 2017.
- Daphne Koller and Nir Friedman. *Probabilistic graphical models: principles and techniques*. MIT press, 2009.
- Kevin B Korb and Ann E Nicholson. *Bayesian Artificial Intelligence*. CRC press, 2010.
- Takeru Miyato, Toshiki Kataoka, Masanori Koyama, and Yuichi Yoshida. Spectral normalization for generative adversarial networks. In *Proceedings of the 6th International Conference on Learning Representations (ICLR 2018)*, 2018. URL <https://openreview.net/forum?id=BlQRgziT->.
- Raha Moraffah, Bahman Moraffah, Mansooreh Karami, Adrienne Raglin, and Huan Liu. Causal adversarial network for learning conditional and interventional distributions. *arXiv preprint arXiv:2008.11376*, 2020.
- Alfred Müller. Integral probability metrics and their generating classes of functions. *Advances in applied probability*, 29(2):429–443, 1997.
- Weili Nie, Nina Narodytska, and Ankit Patel. Relgan: Relational generative adversarial networks for text generation. In *International conference on learning representations*, 2018.
- Sebastian Nowozin, Botond Cseke, and Ryota Tomioka. *f*-gan: Training generative neural samplers using variational divergence minimization. *Advances in neural information processing systems*, 29, 2016.
- George Papamakarios, Eric Nalisnick, Danilo Jimenez Rezende, Shakir Mohamed, and Balaji Lakshminarayanan. Normalizing flows for probabilistic modeling and inference. *Journal of Machine Learning Research*, 22(57):1–64, 2021.
- Judea Pearl. *Probabilistic reasoning in intelligent systems: Networks of plausible reasoning*. Morgan Kaufmann Publishers, Los Altos, 1988.
- Moritz Piening and Matthias Chung. Paired wasserstein autoencoders for conditional sampling. *arXiv preprint arXiv:2412.07586*, 2024.
- Patrick Reiser, Marlen Neubert, André Eberhard, Luca Torresi, Chen Zhou, Chen Shao, Houssam Metni, Clint van Hoesel, Henrik Schopmans, Timo Sommer, et al. Graph neural networks for materials science and chemistry. *Communications Materials*, 3(1):93, 2022.
- Victor Garcia Satorras, Emiel Hooeboom, and Max Welling. E (n) equivariant graph neural networks. In *International conference on machine learning*, pages 9323–9332. PMLR, 2021.
- Franco Scarselli, Marco Gori, Ah Chung Tsoi, Markus Hagenbuchner, and Gabriele Monfardini. The graph neural network model. *IEEE transactions on neural networks*, 20(1):61–80, 2008.
- Alessandro Sperduti and Antonina Starita. Supervised neural networks for the classification of structures. *IEEE transactions on neural networks*, 8(3):714–735, 1997.
- David J Spiegelhalter. Learning in probabilistic expert systems. *Bayesian statistics*, 4:447–465, 1992.
- Viktor Stein, Sebastian Neumayer, Nicolaj Rux, and Gabriele Steidl. Wasserstein gradient flows for moreau envelopes of f-divergences in reproducing kernel hilbert spaces. *arXiv preprint arXiv:2402.04613*, 2024.

- Gábor J. Székely and Maria L. Rizzo. Energy statistics: A class of statistics based on distances. *Journal of Statistical Planning and Inference*, 143(8):1249–1272, 2013.
- Dávid Terjék. Moreau-yosida  $f$ -divergences. In *International Conference on Machine Learning*, pages 10214–10224. PMLR, 2021.
- Boris Van Breugel, Trent Kyono, Jeroen Berrevoets, and Mihaela Van der Schaar. Decaf: Generating fair synthetic data using causally-aware generative networks. *Advances in Neural Information Processing Systems*, 34:22221–22233, 2021.
- Bingyang Wen, Yupeng Cao, Fan Yang, Koduvayur Subbalakshmi, and Rajarathnam Chandramouli. Causal-tgan: Causally-aware synthetic tabular data generative adversarial network. *arXiv preprint arXiv:2104.10680*, 2022.
- Tian Xie and Jeffrey C Grossman. Crystal graph convolutional neural networks for an accurate and interpretable prediction of material properties. *Physical review letters*, 120(14):145301, 2018.
- Depeng Xu, Yongkai Wu, Shuhan Yuan, Lu Zhang, and Xintao Wu. Achieving causal fairness through generative adversarial networks. In *Proceedings of the Twenty-Eighth International Joint Conference on Artificial Intelligence*, 2019.
- Jiaxuan You, Rex Ying, Xiang Ren, William Hamilton, and Jure Leskovec. Graphrnn: Generating realistic graphs with deep auto-regressive models. In *International conference on machine learning*, pages 5708–5717. PMLR, 2018.
- Jiahui Yu, Zhe Lin, Jimei Yang, Xiaohui Shen, Xin Lu, and Thomas S Huang. Free-form image inpainting with gated convolution. In *Proceedings of the IEEE/CVF international conference on computer vision*, pages 4471–4480, 2019.

## A BACKGROUND AND PROPERTIES OF MEASURES OF DISCREPANCY

This appendix collects background definitions and auxiliary facts used in the main text. In particular, we record the notions of determining, admissible, and strictly admissible function classes used in Section 3.

**Definition A.1** ( $\mathcal{P}(\mathcal{X})$ -determining set). A set  $\Gamma \subset C_b(\mathcal{X})$  will be called  $\mathcal{P}(\mathcal{X})$ -determining set if for all  $Q, P \in \mathcal{P}(\mathcal{X})$ ,

$$\int \varphi Q(dx) = \int \varphi P(dx) \quad \forall \varphi \in \Gamma \quad \text{implies} \quad Q = P.$$

**Definition A.2** (Admissible set). Let  $\Gamma \subset C_b(\mathcal{X})$  be equipped with the subspace topology inherited from the weak topology. We say that  $\Gamma$  is *admissible* if it satisfies the following conditions:

1.  $\Gamma$  is convex and closed;
2.  $\Gamma$  is symmetric, i.e.,  $g \in \Gamma$  implies  $-g \in \Gamma$ , and it contains all constant functions;
3.  $\Gamma$  is determining for  $\mathcal{P}(\mathcal{X})$ , i.e., for any  $\mu, \nu \in \mathcal{P}(\mathcal{X})$  with  $\mu \neq \nu$ , there exists  $g \in \Gamma$  such that

$$\int_{\mathcal{X}} g d\mu \neq \int_{\mathcal{X}} g d\nu.$$

**Definition A.3** (Strictly admissible set).  $\Gamma$  will be called *strictly admissible* if it also satisfies the following property: there exists a  $\mathcal{P}(\mathcal{X})$ -determining set  $\Psi \subset C_b(\mathcal{X})$  such that for all  $\varphi \in \Psi$  there exist  $c \in \mathbb{R}$  and  $\varepsilon > 0$  such that  $c \pm \varepsilon\varphi \in \Gamma$ .

## B SUPPORTING MATERIAL

In this section, we prove the auxiliary statements used in Section 5.2 for the Lipschitz discriminator setting. We present the argument first for the simple graph structure in (11), since the argument extends directly to any DAG  $G$  without essential modification.

The next calculation explains why a Lipschitz dependence of the generator on the conditioning variables leads naturally to a Wasserstein-Lipschitz family of conditional distributions. Let  $(\mathcal{Z}, \mathcal{F}, \nu)$  be a probability space,  $\mathcal{X}_{\text{Pa}(i)} \subset \mathbb{R}^m$  and  $g : \mathcal{X}_{\text{Pa}(i)} \times \mathcal{Z} \rightarrow \mathbb{R}^d$ . We assume that for every  $\mathbf{x}_{\text{Pa}(i)} \in \mathcal{X}_{\text{Pa}(i)}$ , the map  $z \mapsto g(\mathbf{x}_{\text{Pa}(i)}, z)$  is measurable and  $g(\mathbf{x}_{\text{Pa}(i)}, \cdot)_{\#} \nu \in \mathcal{P}_1(\mathbb{R}^d)$ , and for any  $\mathbf{x}_{\text{Pa}(i)}, \mathbf{x}'_{\text{Pa}(i)} \in \mathcal{X}_{\text{Pa}(i)}$  and all  $z \in \mathcal{Z}$ ,  $\|g(\mathbf{x}_{\text{Pa}(i)}, z) - g(\mathbf{x}'_{\text{Pa}(i)}, z)\| \leq C d_{\mathcal{X}_{\text{Pa}(i)}}(\mathbf{x}_{\text{Pa}(i)}, \mathbf{x}'_{\text{Pa}(i)})$ . Then, a measurable generator with finite first moment and uniform Lipschitz dependence on the conditioning random vector induces a  $W_1$ -Lipschitz family of conditional distributions.

We begin by verifying this claim in the simplest nontrivial case, namely the terminal conditional distribution in the chain (11).

$$\begin{aligned}
 & W_1(Q(x_3 | X_2 = x_2), Q(dx_3 | X_2 = x'_2)) \\
 &= \sup_{f \in \text{Lip}_b^1(\mathcal{X}_3)} \left\{ \int_{\mathcal{X}_3} f(x_3) Q(dx_3 | X_2 = x_2) - \int_{\mathcal{X}_3} f(x_3) Q(dx_3 | X_2 = x'_2) \right\} \\
 &= \sup_{f \in \text{Lip}_b^1(\mathcal{X}_3)} \left\{ \int_{\mathcal{X}_3} f(x_3) g(x_2, \cdot)_{\#} \nu(dz) - \int_{\mathcal{X}_3} f(x_3) g(x'_2, \cdot)_{\#} \nu(dz) \right\} \\
 &= \sup_{f \in \text{Lip}_b^1(\mathcal{X}_3)} \left\{ \int_{\mathcal{Z}} f(g(x_2, z)) \nu(dz) - \int_{\mathcal{Z}} f(g(x'_2, z)) \nu(dz) \right\} \\
 &\leq \int_{\mathcal{Z}} \|g(x_2, z) - g(x'_2, z)\| d\nu(z) \\
 &\leq C d_{\mathcal{X}_2}(x_2, x'_2)
 \end{aligned}$$

The proof of  $W_1(Q(dx_2 | X_1 = x_1), Q(dx_2 | X_1 = x'_1)) \leq C d_{\mathcal{X}_1}(x_1, x'_1)$  goes similarly.

We now formalize the preceding observation in a proposition that is used to verify condition **(C)** for Lipschitz-bounded discriminator classes.

**Proposition B.1.** *Let  $Q \in \mathcal{P}^G$  and  $G$  is given by (11). Suppose that the map  $\mathbf{x}_{\text{Pa}(i)} \rightarrow Q(dx_{V(i)} | \mathbf{X}_{\text{Pa}(i)} = \mathbf{x}_{\text{Pa}(i)})$ ,  $i \in V$  is  $C$ -Lipschitz with respect to 1-Wasserstein metric, respectively, i.e., for any  $\mathbf{x}_{\text{Pa}(i)}, \mathbf{x}'_{\text{Pa}(i)} \in \mathcal{X}_{\text{Pa}(i)}$*

$$W_1(Q(dx_i | \mathbf{X}_{\text{Pa}(i)} = \mathbf{x}_{\text{Pa}(i)}), Q(dx_i | \mathbf{X}_{\text{Pa}(i)} = \mathbf{x}'_{\text{Pa}(i)})) \leq C \cdot d_{\mathcal{X}_{\text{Pa}(i)}}(\mathbf{x}_{\text{Pa}(i)}, \mathbf{x}'_{\text{Pa}(i)}). \quad (25)$$

If  $\Gamma^L = \text{Lip}_b^L(\mathcal{X})$ , then condition **(C)** holds with  $L_i = L + C$ .

*Proof.* Let  $\gamma \in \Gamma$ . To show that **(C)** holds, we prove that for any pairs  $(x_i, \mathbf{x}_{\text{Pa}(i)})$  and  $(x'_i, \mathbf{x}'_{\text{Pa}(i)}) \in \mathcal{X}_{i \cup \text{Pa}(i)}$

$$|I_{i, \text{Pa}(i)}[\gamma](x_i, \mathbf{x}_{\text{Pa}(i)}) - I_{i, \text{Pa}(i)}[\gamma](x'_i, \mathbf{x}'_{\text{Pa}(i)})| \leq L \cdot d_{\mathcal{X}_i \times \mathcal{X}_{\text{Pa}(i)}}((x_i, \mathbf{x}_{\text{Pa}(i)}), (x'_i, \mathbf{x}'_{\text{Pa}(i)})).$$

We start from the left-hand side of the above inequality for  $i = 3$  and  $\text{Pa}(i) = \text{Pa}(3) = 2$ , and bound as follows: Let  $\gamma(\mathbf{x}) = \gamma(x_1, x_2, x_3)$

$$\begin{aligned}
 & |I_{3,2}[\gamma](x_3, x_2) - I_{3,2}[\gamma](x'_3, x'_2)| \\
 &= \left| \int_{\mathcal{X}_1} \gamma(\mathbf{x}) Q(dx_1 | X_2 = x_2) - \int_{\mathcal{X}_1} \gamma(\mathbf{x}') Q(dx_1 | X_2 = x'_2) \right| \\
 &= \int_{\mathcal{X}_1} \int_{\mathcal{X}_1} |\gamma(\mathbf{x}) - \gamma(\mathbf{x}')| Q(dx_1 | X_2 = x_2) Q(dx_1 | X_2 = x'_2) \\
 &= \int_{\mathcal{X}_1} \int_{\mathcal{X}_1} L d_{\mathcal{X}}(\mathbf{x}, \mathbf{x}') \pi_{x_2, x'_2}(dx_1) \\
 &\leq L \cdot d_{\mathcal{X}_3 \times \mathcal{X}_2}((x_2, x_3), (x'_2, x'_3)) \\
 &\quad + W_1(Q(dx_1 | X_2 = x_2), Q(dx_1 | X_2 = x'_2))
 \end{aligned}$$

where  $\pi_{x_2, x'_2}$  is any coupling of  $Q(dx_1 | X_2 = x_2)$  and  $Q(dx_1 | X_2 = x'_2)$ . The result follows immediately. We work similarly  $I_1[\gamma]$  and  $I_{2,1}[\gamma]$ .  $\square$